Full length article

Air pollution mapping and variability over five European cities

Karine Sartelet [a],[*] , Jules Kerckhoffs [b] , Eleni Athanasopoulou [c] , Lya Lugon [a] ,
Jeni Vasilescu [f] , Jian Zhong [e],[j] , Gerard Hoek [b] , Cyril Joly [d] , Soo-Jin Park [a] ,
Camelia Talianu [f],[h] , Sef van den Elshout [k] , Fabrice Dugay [d] , Evangelos Gerasopoulos [c] ,
Alexandru Ilie [f],[g] , Youngseob Kim [a] , Doina Nicolae [f] , Roy M. Harrison [e] , Tuukka Petäjä [i]

[a] *CEREA, Ecole des Ponts, Institut Polytechnique de Paris, EdF R&D, IPSL, 77 455 Marne-la-Vallée, France*
[b] *Institute for Risk Assessment Sciences, Utrecht University, Utrecht, The Netherlands*
[c] *Institute for Environmental Research and Sustainable Development, National Observatory of Athens 15236 Athens, Greece*
[d] *Airparif, Paris, France*
[e] *School of Geography, Earth & Environmental Sciences, University of Birmingham, Edgbaston, Birmingham B15 2TT, UK*
[f] *National Institute of Research and Development for Optoelectronics-INOE 2000, 077125 Măgurele, Romania*
[g] *Faculty of Geography, University of Bucharest 010041 Bucharest, Romania*
[h] *Institute of Meteorology and Climatology, Department of Water, Atmosphere and Environment, University of Natural Resources and Life Sciences, A-1180 Vienna,
Austria*
[i] *Institute for Atmospheric and Earth System Research/Physics, University of Helsinki 00014 Helsinki, Finland*
[j] *Computational Science and Engineering Group, University of Greenwich, Old Royal Naval College, Park Row, London SE10 9LS, UK*
[k] *DCMR, Environmental Protection Agency, Schiedam, The Netherlands*

ARTICLE INFO

ABSTRACT

Mapping urban pollution is essential for assessing population exposure and addressing associated health impacts. High urban concentrations are due to the proximity of sources such as traffic or residential heating, and to urban density with the presence of buildings that reduce street ventilation. This urban complexity makes fine-scale mapping challenging, even for regulated pollutants such as NO_2 and $PM_{2.5}$. In this study we apply state-of-the-art empirical and deterministic modeling approaches to produce high-resolution (<100 m) pollution maps across five European cities (Paris, Athens, Birmingham, Rotterdam, Bucharest). These methodologies enable full-city mapping capturing intra-urban gradients of concentrations. Depending on the methodology, regulated pollutants (NO_2, $PM_{2.5}$) and/or emerging pollutants (black carbon (BC) and ultrafine particles (UFP characterized here by particulate number concentration PNC)) are considered. For deterministic modelling, different approaches are presented: a multi-scale Eulerian modelling chain down to the street scale with chemistry/aerosol dynamics at all scales, multi-scale hybrid models with Eulerian regional dispersion and Gaussian subgrid dispersion, and a Gaussian-based model. Empirical land use regression models were developed based upon mobile monitoring.

To compare the relative performance of the methodologies and to evaluate their performance and limitations, the modelling results are compared to fixed measurement stations. We introduce a standardized metric to quantify spatial and seasonal variability and assess each method's capacity to reproduce fine-scale urban heterogeneity. We also evaluate how data assimilation affects both concentration accuracy and variability representation—particularly relevant for emerging pollutants where measurement data are sparse. We confirm established seasonal and spatial patterns: spatial variability is more pronounced for PNC, NO_2 and BC than $PM_{2.5}$, and concentrations are higher during the winter periods. We also observe reduced spatial variability in winter for $PM_{2.5}$ (linked to residential heating) and for BC in cities with significant wood burning emissions. This study adds unique value by evaluating these patterns using fixed measurement stations, and quantifying them across entire urban areas at very fine spatial resolution (<100 m). Furthermore, important methodological strengths and limitations are pointed out, providing practical guidance for the selection and improvement of urban exposure mapping methods, supporting the implementation of the new EU Air Quality Directive.

1. Introduction

The global impact of outdoor air pollution on health is very high (Brauer et al. 2024). The World Health Organization (WHO) estimates that air pollution is responsible for 6 to 7 million premature deaths a year worldwide, and 300 000 in Europe. It is the fourth leading health risk factor worldwide. A large part of the health impacts is attributed to particles (Cohen et al. 2015, Southerland et al., 2022). Nevertheless, particles of varying sizes and characteristics impact health differently (Park et al., 2018; Schraufnagel, 2020; World Health Organization, 2021a). While the effects of fine particles expressed as $PM_{2.5}$ are well-established, resulting in guidelines values by WHO, the evidence for health effects of black carbon (BC) and ultrafine particles (UFP) is judged less certain by WHO (WHO, 2021). BC and UFP are considered as emerging pollutants (WHO 2021b, Goobie et al. 2024). Thus, they should now be monitored at different sampling sites following the recent European Directive 2024/2881. Long-term UFP and BC exposure was shown to be associated with natural and lung cancer mortality among adults independently from other regulated air pollutants (Lequy et al 2021, 2023, Bouma et al. 2023). Strong gradients of concentrations are particularly observed in urban environments for these emerging pollutants (Llyod et al. 2023, Park et al. 2024), whose concentrations are there strongly influenced by road traffic (Ridolfo et al. 2024). The population exposure to outdoor concentrations is strongly influenced by these local variabilities, with larger differences for NO_2 than for $PM_{2.5}$ (Lugon et al. 2022, Wang et al. 2024). Although the new Air Quality Directive explicitly recognizes modeling applications as valuable tools for informing air quality plans and roadmaps, accurately modeling the sharp gradients between roads and urban background for NO_2 remains challenging, with many models struggling to do so, as recently noted by de Meij et al. (2024) for CAMS (Copernicus Atmosphere Monitoring Service) models (Colette et al. 2024). This challenge is even more pronounced for black carbon (BC) and ultrafine particles, which are still rarely represented in modelling frameworks.

One of the main objectives of the RI-URBANS European project (https://riurbans.eu/) is to bring accessible service tools to enhance air quality monitoring networks, including evaluating air pollution exposure. To assess the population exposure to pollutants, mapping is required at spatial scales below 100 m, at the minimum at the annual average scale but preferably at shorter time scale, in order to assess short-term exposure to those pollutants. The precision of spatial and seasonal variability representation directly determines the accuracy of exposure characterization. Given that different pollutants may exert distinct health effects it is important to determine techniques to map for accurately mapping all pollutants of interest. Fine-scale inter-comparisons usually focus on a district rather than a city, and meteorology or NO_2 comparisons rather than multi-pollutant assessments (Thouron et al. 2019, Martin et al. 2024). Different mapping techniques exist: from empirical techniques using fixed-site or mobile measurements and Land-Use-Regression (LUR) modelling (Apte and Manchanda 2024, Ma et al. 2024) to deterministic modelling (Lugon et al. 2022, Patino et al. 2024, Sartelet et al. 2024). Deterministic modelling may involve different scales, from regional to local scales, and can be used in synergy with statistical approaches to assess local concentration gradients (Valari

et al. 2010, Squarcioni et al. 2024). Mapping fine-scale urban heterogeneities is challenging, especially for emerging pollutants, for which tools have only been recently developed (Kerckhoffs et al 2022b, Park et al. 2024). Furthermore, it requires extensive input data—such as mobile measurements for LUR or detailed fine-scale emission inventories for deterministic modeling. Evaluation of the validity of maps of modelled air pollutant concentrations across cities is also challenging because of the generally spatially sparse monitoring data. The difficulty lies in evaluating the models at different types of stations characteristic of urban areas (traffic, urban background, suburban). This applies to regulated pollutants such as NO_2 and $PM_{2.5}$ in most cities, but even more to the emerging pollutants UFP and BC, for which routine monitoring is still scarce. We can evaluate however whether the models broadly represent the measurements at the few monitoring sites that are typically available in cities. The simulated concentrations may be corrected using ground-based observations and algorithms based on spatial interpolation techniques such as kriging (Shukla et al. 2020), or data-assimilation techniques (Tilloy et al. 2013).

Rather than intending a harmonized modelling inter-comparison, this study aims to benchmark current empirical and deterministic methodologies under the operational constraints faced by cities. The wide range of modelling techniques across cities and variability in the pollutant modelled reflects both the realities of data availability and the emerging nature of tools for fine-scale mapping of pollutants. Hence, this study aims to compare state-of-the-art mapping techniques (empirical and deterministic modeling) in capturing the spatial and seasonal variability of air pollutants (NO_2, $PM_{2. 5}$, black carbon, and ultrafine particles), provided the technique supports their modeling. The evaluation of the accuracy of methods in representing spatial and temporal variation is crucial to provide insights in their effectiveness in estimating population exposure.

The different mapping techniques used here (Land-Use Regression and deterministic multi-scale modelling) are presented in section 2. The statistics used to evaluate modelled concentrations, assess variability and integrate across cities are detailed in section 3. The models' setup and comparisons of concentrations to measurements are detailed in section 4. Section 5 presents the assessment of seasonal and spatial variability, along with their evaluation using fixed station measurements.

2. Mapping techniques

Different techniques may be used to provide high-resolution outdoor exposure city maps for pollutants. Techniques based on Land-Use Regression with mobile measurements and deterministic modelling have been used in this work.

2.1. Land-Use Regression models

In epidemiological studies of long-term air pollution exposure, land-use regression (LUR) models are often used (Hatzopoulou et al., 2017; Hoek, 2017; Jerrett et al., 2005; Ma et al., 2024) to determine the concentrations to which people are exposed. They are usually based on multiple linear regression using measurements from fixed monitoring stations, passive sampling or more recently mobile monitoring, and land-use features that can explain the variation in those measurements (Ma et al. 2024). An extension of this approach is a mixed-effect model, which uses fixed effects estimated from a linear regression model and random intercepts for all individual street segments (random-effect). The mixed effect model finetunes the prediction of the fixed-effect LUR model based on the measured between and within-street segment concentration variation. The mixed-effect modelling framework has been applied to develop high-resolution NO_2, UFP and BC concentration maps for Amsterdam and Copenhagen based on mobile monitoring with better performance than data-only and LUR-only approaches (Kerckhoffs et al. 2022, Kerckhoffs et al, 2022b).

The required input data are measurement data and land-use predictor variables, such as land cover, population density on a specific area, road network and traffic intensity. Land cover and land use of terrain may be obtained from the CORINE dataset (European Environment Agency, 2018), while the population density may be obtained from national or European statistics catalogues. The road network along with traffic intensity variables may be obtained from the national statistics, if available, but can be also calculated using an available repository such as Open Street Maps (OpenStreetMap, 2021). Measured concentrations are provided for each road segment. They are averaged in time over the period studied. The same spatial resolution is used all-over the area, the concentrations are computed using the regression coefficients (Kerckhoffs et al. 2022, Kerckhoffs et al., 2024).

2.2. Deterministic models

Techniques based on deterministic modelling may also be used to provide high-resolution outdoor exposure city maps. They usually require an emission inventory, meteorological data and a model that estimates the evolution of concentrations in the atmosphere due to chemical and physical transformations. At the regional scale, Eulerian chemical transport models are often used for forecasting, scenarios, or to assess health effects (Adelaide et al 2021). The simulated domain is discretized into cells of fixed size and the concentrations of the pollutants are assumed homogeneous in each grid cell. They typically have horizontal resolutions coarser than 1 km^2. To represent the locally high concentrations, local-scale models account for the dispersion and sometimes the chemical transformation of the pollutants in the vicinity of their emissions. Different approaches may be used to represent the local dispersion. The computational fluid dynamics approach is the most complex and accurate: the simulated domain is discretized in a Eulerian way and the flow is explicitly solved (Moin and Mahesh 1998), leading to a detailed representation of dispersion even when buildings are present. Closure schemes may be used to represent the variations of the fluctuations of the flow, such as Large Eddy Simulation or Reynolds-averaged Navier–Stokes (Salim et al. 2011). These approaches require large computational time, limiting the domain and period of study, especially if chemistry and aerosol dynamics are taken into account (Lin et al. 2023, 2024).

2.2.1. Local-scale Gaussian-based models

To reduce computing time, Gaussian models are widely used, assuming that the dispersion of pollutants follows a Gaussian law (Hood et al. 2014, Rood 2014, Karl et al. 2019, Denby et al. 2020, Fernandes et al. 2021), which characteristics depend on the wind and atmospheric stability. Although this approach may be well suited to represent flat terrain, it is not designed to represent built or irregular domains (Patino et al. 2024, Martin et al. 2024), and adaptations of the Gaussian law have been proposed (Bercowitz 2000, Hood et al. 2021). For example, in the ADMS-Urban model, a street canyon module was added to represent the circulation of air flow for street canyon environments (Hood et al., 2021). These approaches based a Gaussian representation of the local flow only deal with simple chemistry scheme, often assuming particles to be inert (Patino et al. 2024), and they may need some adaptations to be coupled to Eulerian chemical transport models (CTM) (Hood et al. 2018; Denby et al. 2020), in order to avoid double counting of emissions that could occur if the regional and local concentrations are just added. For example, in EPISODE City-Chem, a time-stepping scheme that differentiates the local and regional contributions is used (Hamer et al. 2020). Furthermore, the assumption of homogeneity required in Gaussian plume is challenged in an urban environment, because the length of roughness varies greatly with the different heights of blocks of flats, the different widths of streets, avenues, boulevards, green spaces and squares. The Gaussian-based local-scale models are often gridded on a grid of size ranging from 10 m x 10 m to 100 m x 100 m.

2.2.2. Local-scale street-network models

To avoid the tricky coupling between a local Gaussian model and a regional model, a Eulerian approach may be used at the local-scale in urban areas composed of streets. Those are then explicitly meshed. The concentrations are often assumed to be uniform in each street segment, or discretized with a few vertical levels (Kim et al., 2022; Sarica et al., 2023). In these street-network models, the flow inside streets and the exchange between the street and the above canopy are parameterized depending on the meteorology and the street characteristics, using wind-tunnel experiments or computational fluid dynamics simulations (Maison et al., 2022a; Soulhac et al., 2009), potentially considering the effects of street trees (Maison et al. 2022b). In the street-network model MUNICH, the street-network is discretized into street segments, which exchange between them, as well as with the urban background using a Eulerian approach and parameterized local meteorology. The regional-scale concentrations are boundary conditions of the street-scale concentrations, allowing to have a continuity in the modelling of dispersion, chemical transformations and aerosol dynamics at all scales (Lugon et al. 2021).

In terms of input data, for the regional-scale modelling, CTM require several input data that are specific to the domain of study: meteorology, boundary conditions, emission inventory. Meteorological fields may be obtained by different agencies, such as ECMWF (European Centre for Medium-Range Weather Forecasts), NCEP (National Centers for Environmental Prediction), and downscaling down to the urban scale may be performed using different models, such as WRF (Weather Research & Forecasting Model). Boundary conditions may be obtained from global models or regional reanalysis, such as those provided by CAMS (Copernicus Atmosphere Monitoring Service), and/or from a nested domain approach down to the city scale. Emission inventories using a top-down approach are available at the European scale (e.g. EMEP, CAMS), and they may be downscaled to the city scale. Tools for this purpose may be embedded in chemistry-transport models (e.g. CHIMERE, Menut et al. 2021), or use a spatial disaggregation method, for example based on developments of the UrbEm tool (Ramacher et al. 2021) for the European CAMS-REG emission inventory. Bottom-up inventories may also be used.

For local-scale modelling, hourly road-network emissions are needed. Correction of the traffic flow and hence of the traffic emissions using traffic count loops may improve the modelling for some pollutants, such as BC and PNC concentrations (Park et al 2024). For street-network models, not only emissions, but also the characteristics of the main streets (lengths, widths and heights) are necessary for local-scale simulations. Concentrations of the different pollutants are output hourly, with a spatial resolution of 1 km^2 (or more) for the urban background concentrations from the CTMs. The street-network models provide concentrations in each street segment of the network.

2.3. Deterministic models with data assimilation

The simulated concentrations may be corrected using data assimilation techniques. Here, a technique based on the BLUE (best linear unbiased estimator) algorithm of Tilloy et al. (2013) is presented. The assimilated concentrations are linearly dependent on the simulated concentrations and the observations, and their estimations require the estimation of the state errors covariance matrix B and the observational errors covariance matrix R. The covariance matrix B represents the uncertainty in the estimate of the concentrations. Here, it is expressed, such as incorporating model properties, and more specifically, the simulated concentrations x_i^b and x_j^b at grid points i and j, respectively:

$$B_{i,j} = \varphi\left(x_i^b\right)\varphi\left(x_j^b\right)exp^{-d_{i,j}/d_0} \tag{1}$$

where $\varphi(x) = \varphi_0 + x$, with $\varphi_0 > 0$, and $d_{i,j}$ represents the Euclidean distance between the grid points, and $d_0 > 0$ is a characteristic distance

scale. The retained values for these parameters are $d_0 = 75$ km and $\varphi_0 = 10$ μg/m^3, which allows to adapt the error covariance to the local pollution conditions.

This formulation brings several notable advantages. First, the prior variance is non-uniform, as it increases with the simulated concentration x^b, reflecting higher uncertainty in regions with elevated pollution levels, such as near major traffic routes. This feature ensures that areas with more significant pollution are treated with appropriately greater uncertainty. Second, the model effectively captures spatial heterogeneity by tailoring the uncertainty to the local characteristics of the environment. This represents a significant improvement over the uniform treatment of road segments that characterized the approach by Tilloy et al. (2013). Moreover, the exponential decay factor $e^{-d_{i,j}/d_0}$ ensures that correlations diminish with distance, progressively reducing long-distance correlations and eliminating them at larger distances, thereby preventing spurious correlations between distant points. The constructed covariance matrix B is symmetric and positive semi-definite, which preserves the essential mathematical properties required for data assimilation.

The observation uncertainty is modelled through a diagonal observation covariance matrix R, which is defined as

$$R = r_0 HBH^T \tag{2}$$

where $0 < r_0 < 1$, ensuring that the observation uncertainty is lower than the model uncertainty at each grid point. Here, the value $r_0 = 0.05$ is retained, providing a suitable balance between model and observation uncertainties.

Since both the background covariance matrix B and the observation covariance matrix R are functions of the simulated concentrations x^b, they change dynamically every hour. The assimilation process is conducted every hour using hourly available measurement data, which means that both B and R are updated at each assimilation step to reflect the latest pollution levels.

To assess the accuracy of the assimilation system, cross-validation was performed using the leave-one-out method every hour (not shown here). For each measurement station, an analysis is performed excluding the observation from that station, using the remaining available measurements. Given the computational intensity of this process, the fast computation formula was used for cross-validation to reduce computational time while maintaining the robustness of the evaluation.

2.4. Mapping techniques and pilot cities

The different approaches presented above are used to estimate pollutant concentrations and variabilities over different European cities (Paris, Birmingham, Athens, Rotterdam and Bucharest). They are summarized in Table 1.

For deterministic modelling, four models based on different methodologies and complexity are used:

- Multi-scale Eulerian modelling over Paris with the CHIMERE/MUNICH/SSH-aerosol modelling chain. It is a 3-dimensional (3-D) Eulerian CTM grid model with sub-grid Eulerian dispersion and chemistry/aerosol dynamic at all scales (Maison et al. 2024, Park et al. 2024).
- Multi-scale hybrid modelling with the Episode-CityChem modelling chain over Athens and the CHIMERE/ADMS modelling chain over Paris. They are 3-D Eulerian CTM grid model with sub-grid Gaussian dispersion (Karl et al. 2019, Lasne et al. 2023).
- The Gaussian-based model ADMS-Urban over Birmingham (Zhong et al. 2023)

The mixed-effect LUR model (Kerckhoffs et al. 2022) is used over Rotterdam and Bucharest.

3. Methodology for the statistical analysis

3.1. Concentrations

To evaluate the modelled concentrations, for regulated pollutants (NO$_2$ and PM$_{2.5}$), the yearly Modelling Quality Indicator (MQI, Janssen and Thunis, 2022) for the 95th percentile is determined (Fig. 1). It corresponds to the difference between the measured and observed concentrations normalised by the measurement uncertainty and by a coefficient β of 2. The quality of the modelling is good for MQI < 1, which reflects that the model bias is less than twice the measurement uncertainty. Yearly concentrations are here approximated by averaging seasonal concentrations. MQI at each fixed measurement stations and for each season are shown in Appendix. For deterministic modelling, hourly concentrations are also evaluated in the Appendix by comparison to fixed measurement stations using the Mean Fractional Bias (MFB), Mean Fractional Error (MFE), and the fraction 2 (FAC2), representing strict and less strict criteria for model evaluation[1] (Boylan and Russell 2006, Hanna and Chang 2012).

To integrate concentrations over the cities, the average modelled concentrations $\overline{C_{loc}}$ is estimated by averaging concentrations over grid cells:

$$\overline{C_{loc}} = \frac{1}{n}\sum_i C_{loc}(i) \tag{3}$$

where n is the number of cells, and $\overline{C_{loc}}(i)$ is the local concentration in the cell i. For deterministic modelling based on sub-grid Gaussian dispersion, the surfaces range between 50 x 50 m^2 and 100 x 100 m^2. For the street-network model and the mixed-effect LUR model, the concentrations are averaged over the different street segments, rather than grid cells.

3.2. Variability

Urban variabilities are quantified using coefficients of variation, specifically the normalized standard deviation (NSD), which is calculated to represent either seasonal or spatial variability. For NO$_2$ and PM, the Model Performance Indicator (MPI) proposed by de Meij et al. (2025) is also studied.

3.2.1. Spatial variability

The spatial sub-grid variability within a regional model grid, averaged over the time, can be characterized by the NSD of the sub-grids within the grid. Each city is meshed using a regular 1 km^2 grid. For each mesh of the 1 km^2 grid, the NSD can be used to indicate and quantify the difference between the sub-grid or street concentrations and the mean value:

$$NSD = \frac{\sqrt{\frac{1}{n}\sum_i (C_{loc}(i) - \overline{C_{loc}})^2}}{\overline{C_{loc}}} \tag{4}$$

where $\overline{C_{loc}}(i)$ is the local concentration in the subgrid or street i,

$\overline{C_{loc}}$ is the mean concentrations of the sub-grids and n the total number of sub-grids/streets within the 1 km^2 grid. Maps of NSD for the different pollutants are shown in Appendix B.

The variability is also characterized over the whole city in the Table Appendix C and in Fig. 8. These averages are computed by summing i in equation (4) over all grid mesh located in the considered area. The higher the NSD, the more variability of the concentrations, indicating the strong influence of highly localized sources such as traffic.

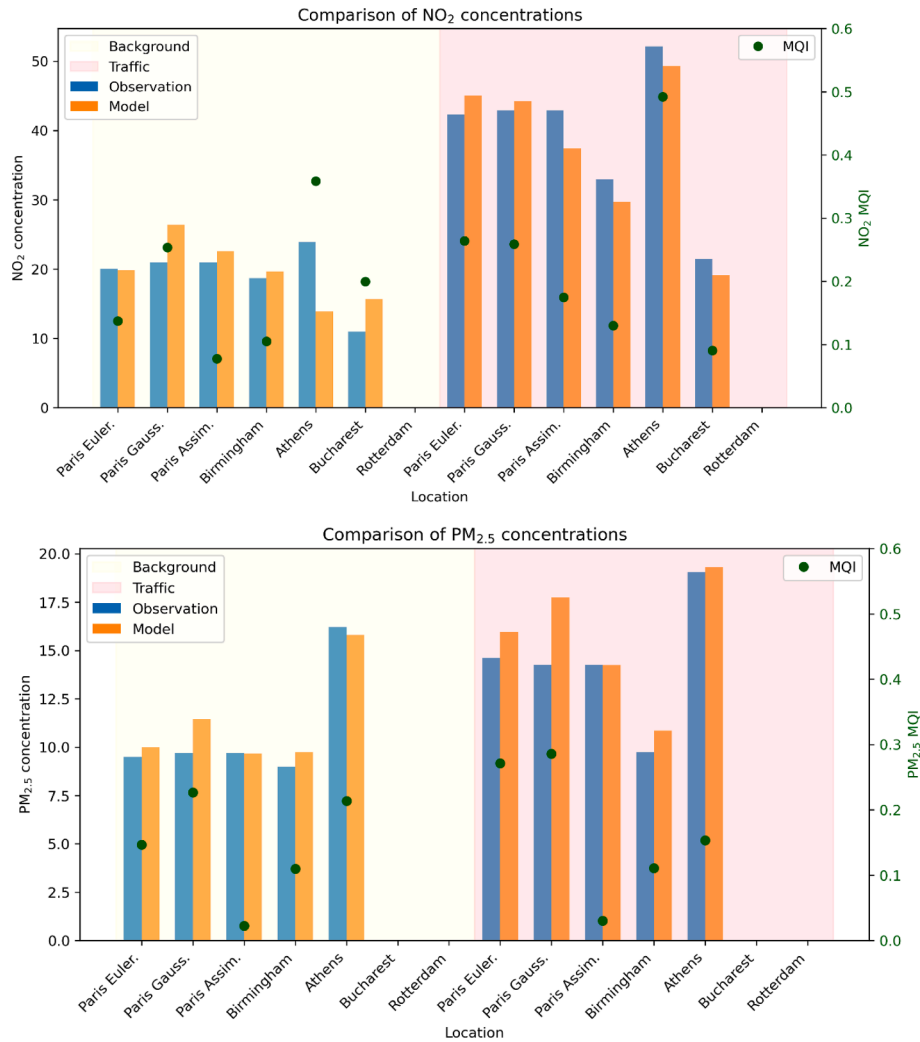To enable a comparison of variability between the model and mea-

---

[1] Strict: MFE < 50%, |MFB| < 30%, FAC2 > 50%, Less strict: MFE < 75%, |MFB| < 50%, FAC2 > 30%.

Table 1

Summary of the mapping methodologies used in each pilot city, as well as the pollutant mapped, and pollutants for which fixed urban background and traffic measurements are available.

City/ Method.	Mixed-effect LUR	CHIMERE MUNICH	CHIMERE ADMS	CHIMEREADMS with DA	EPISODE-CityChem	ADMS	Fixed urban meas.	Fixed traffic meas.
Paris		NO_2, $PM_{2.5}$, BC, UFP	NO_2, $PM_{2.5}$, BC	NO_2, $PM_{2.5}$, BC			NO_2, $PM_{2.5}$, BC, UFP	NO_2, $PM_{2.5}$, BC
Athens					NO_2, $PM_{2.5}$		NO_2, $PM_{2.5}$	NO_2, $PM_{2.5}$
Birmingham						NO_2, $PM_{2.5}$, UFP	NO_2, $PM_{2.5}$, UFP	NO_2, $PM_{2.5}$
Rotterdam	NO_2, BC, UFP						NO_2, BC	NO_2, BC
Bucharest	NO_2, PM_{10}, UFP						NO_2, PM_{10}	NO_2, PM_{10}

Fig. 1. Comparisons of NO_2 (upper panel) and $PM_{2.5}$ (lower panel) to fixed-station measurements at urban background and traffic stations. The concentrations are averaged over the winter and summer seasons. The model quality indicator MQI is obtained by averaging the errors over the measurement stations.

surements, the variability between background and traffic concentrations at fixed measurement sites is estimated using both measured and modeled data. Hence, taking $\overline{C_{loc}}$ as the mean concentration at traffic and background sites,

$$\overline{C_{loc}} = \frac{C_{background} + C_{traffic}}{2} \tag{5}$$

Equation (4) may then be rewritten as

$$NSD_{stat} = \frac{\sqrt{\frac{1}{2}\left(\left(C_{background} - \overline{C_{loc}}\right)^2 + \left(C_{traffic} - \overline{C_{loc}}\right)^2\right)}}{\overline{C_{loc}}} \tag{6}$$

This NSD at stations quantifies the variability between background and traffic measurement sites. The variability is estimated using either the measured concentrations or the modelled data (Observed Stations NSD and Modelled Stations NSD), and the resulting values are compared to assess consistency between observations and model outputs. Note that the variability integrated over a city is expected to be lower than the variability between concentrations at background and traffic stations, as

it may be more or less pronounced depending on the area's specific contrasts between background and traffic influences.

For NO$_2$ and PM$_{2.5}$, the MPI of deMeij et al. (2025) is also estimated by computing the differences between measured and modelled gradients of concentrations between urban background and traffic measurement sites. These differences are normalised by the measurement uncertainty, which value is representative of the maximum allowed measurement uncertainty, and by a coefficient β of 2. The quality of the modelling is good for MPI < 1, which reflects that the model bias is less than twice the measurement uncertainty.

3.2.2. Seasonal variability

Similarly to the spatial NSD, the seasonal NSD is estimated by calculating the coefficient of variation between summer and winter:

$$NSD_{seas} = \frac{\sqrt{\frac{1}{2}((C_{summer} - \overline{C_{seas}})^2 + (C_{winter} - \overline{C_{seas}})^2)}}{\overline{C_{seas}}} \quad (6)$$

with $\overline{C_{seas}}$ the mean concentration between summer and winter.

For NO$_2$ and PM$_{2.5}$, the MPI of deMeij et al. (2025) is also estimated by computing the differences between measured and modelled gradients of concentrations between winter and summer at measurement sites.

These differences are normalised by the measurement uncertainty and by a coefficient β of 2. As for the spatial variability, the quality of the modelling is good for MPI < 1.

4. Models' set-up and evaluation of the modelled concentrations

In each pilot city, concentrations are measured and simulated over a winter and a summer period. The modelling set-up is briefly presented for each pilot city, and the modelled concentrations are evaluated by comparison to fixed measurements when possible, and concentrations maps are built over the pilot cities. More detailed concentrations maps and model evaluations are shown in Appendix A.

For the comparisons to fixed measurement stations, the comparison is performed for concentrations averaged over a winter and a summer period in Fig. 1 for NO$_2$ and PM$_{2.5}$ and in Fig. 2 for BC and PNC. The averages of MQI over all stations are shown in Fig. 1, and the detailed statistics per stations are shown in Appendix A. All the models performed well for the modelling of seasonal averages with MQI always lower than 1. Table 2 details the modelled concentrations averaged over the different cities, and Fig. 3 shows the maps of PNC for winter in Paris, Bucharest, Birmingham and Rotterdam. Strong gradients in PNC near roads, highways and industrial areas are observed, because of the
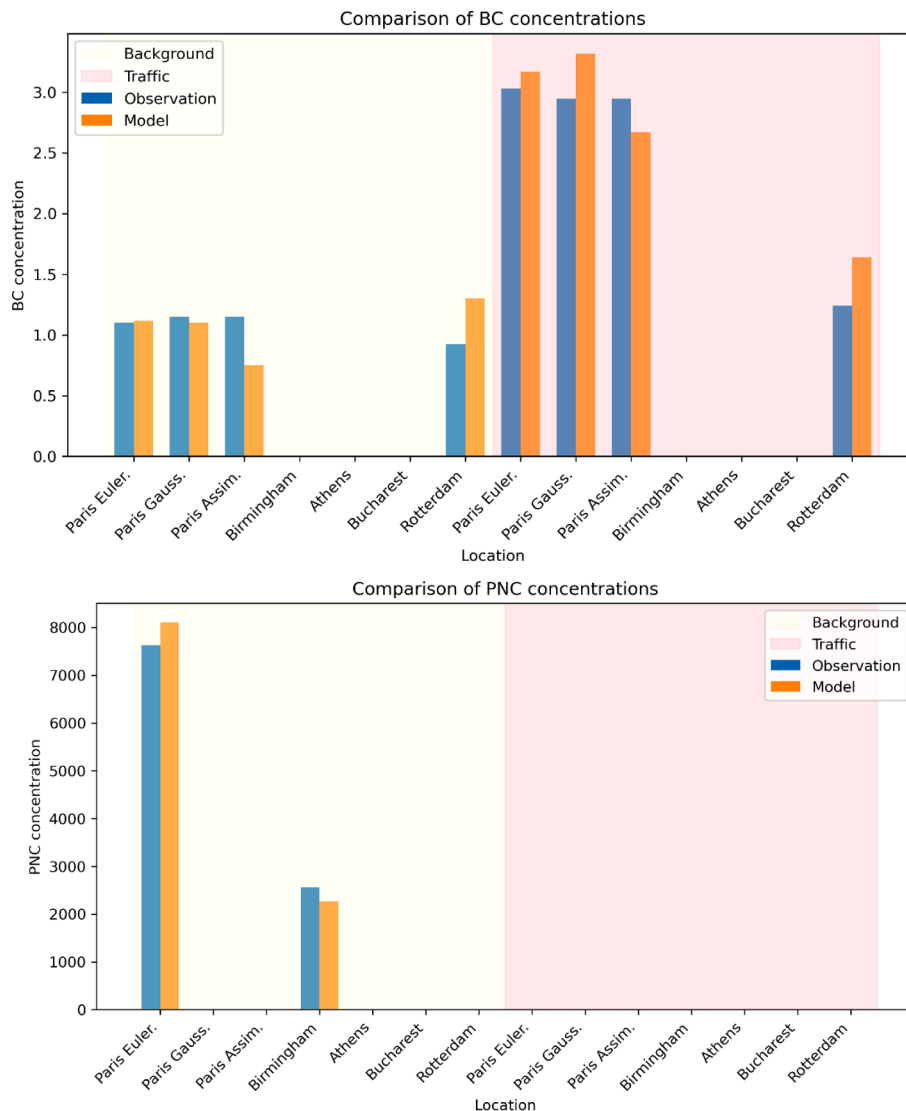
Fig. 2. Comparisons of BC (upper panel) and PNC (lower panel) to fixed-station measurements at urban background and traffic stations. The concentrations are averaged over the winter and summer seasons.

proximity of emission sources and the limited lifetime of ultrafine particles, which grow fast by coagulation and condensation of low-volatile species.

Care should be exercised in making comparisons between cities, as the model formulations and emission factors used in the deterministic models were not the same. However, useful insights can be gained from the within-model evaluations and limited intercomparisons reported below.

4.1. Eulerian approach with the CHIMERE/MUNICH/SSH-aerosol chain over Paris

The Eulerian CHIMERE/MUNICH/SSH-aerosol chain was setup over Paris. The segments of the street network are those defined by Airparif, the Île-de-France air quality agency. They correspond to the main roads. The main street characteristics are obtained from the French BDTOPO database (https://geoservices.ign.fr/bdtopo). The street network is made of 4655 streets and extends over the city of Paris and its nearby suburbs. Regional-scale concentrations are simulated with the CHIMERE model (Menut et al. 2021) coupled to the street network MUNICH (Kim et al., 2022). The concentrations of NO_2, $PM_{2.5}$, PNC, BC and other particle components (e.g. inorganic and organic aerosols) are simulated. All the gas and particle components simulated at the regional scale are also simulated down to the street scale. Indeed, the chain CHIMERE/ MUNICH use the same aerosol module (SSH-aerosol, Sartelet et al. 2020) at both the regional and local scales, allowing it to take into account the dynamic of particles at all scales. In the CHIMERE/MUNICH chain, nested domains are considered using CAMS boundary conditions over Europe. The smallest domain of CHIMERE simulation is discretized with a 1 km^2 resolution over Greater Paris. A zoom is performed in the streets of Paris, which are explicitly represented using a Eulerian approach with the street network MUNICH. The bottom-up Aiparif inventory of the year 2019 is used, except for the traffic fleet and emissions which are specific to the period of simulation (winter 2020 and summer 2022 here). The road traffic emissions data were produced based on the results obtained using the Heaven system. The strength of this system is to use a traffic model that is corrected from the count data received in near real time. In the chain CHIMERE/MUNICH, the regional-scale traffic emissions were estimated by aggregating the local-scale emissions.

Number emissions and the size distribution of emissions were estimated from the emission inventory using the methodology detailed in Sartelet et al. (2022) and Park et al. (2024). The emission inventories provide estimations of $PM_{2.5}$ emissions for the different activity sectors. To distribute $PM_{2.5}$ emissions in the modelled particle size sections, emissions of particles in the range $PM_{0.1}$-PM_1 and $PM_{0.01}$-$PM_{0.1}$ are estimated using the $PM_1/PM_{2.5}$ and $PM_{0.1}/PM_1$ ratios given in Sartelet et al. (2022) (Table A2) for each activity sector. The emissions in each of the size ranges: $PM_{0.01}$-$PM_{0.1}$, $PM_{0.1}$-PM_1, and PM_1-$PM_{2.5}$ are then distributed amongst the model size sections with an algorithm that conserves mass and number. Note that for the residential sector, the lowest diameter considered for emission is 80 nm (against 10 nm for the other sectors).

For comparisons to observations, the simulated BC concentrations are obtained by multiplying the simulated EC concentrations by a harmonization factor, following Savadkoohi et al. (2024). A harmonization factor of 1.79 and 1.70 was determined for Paris in the summer 2022 and the winter 2020/2021 respectively using EC and eBC collocated measurements at Châtelet-les-Halles station, which is an urban background station operated by Airparif in the centre of Paris. The simulation was performed with the set-up detailed in Park et al. (2024) between 2 June 2022 and 31 July 2022 for the summer period, and between 7 December 2020 and 28 February 2021 for the winter period. Particles of diameters between 10 nm and 10 μm were modelled.

The simulated concentrations are evaluated by comparison to measurement stations from the Airparif network, as well as from a Airparif campaign for the winter period 2020/2021. Regional-scale concentrations (in 1 km^2 cells) are compared to measurements at background stations, and street concentrations (in the street cells) are compared to measurements at traffic stations. 24 and 9 background and traffic stations respectively are available to evaluate NO_2 in summer and winter. For $PM_{2.5}$, 10 and 8 background stations are available in the summer and winter, and the number of traffic stations is lower: 3 and 1 in summer and winter. Less stations are available to evaluate BC: 4 background and 2 traffic stations in both winter and summer, while for PNC only background stations are available: 4 in the summer and 5 in the winter. The location of the stations is detailed in Appendix A. The mean NO_2, BC, $PM_{2.5}$ and PNC at urban background stations are higher than the concentrations at traffic sites. As detailed in Appendix A (Tables A.1.1, A.1.2, A.1.3 and A.1.4), the modelled concentrations satisfy the strictest performance criteria for all pollutants (NO_2, BC, $PM_{2.5}$ and PNC) at both background and traffic stations. The average concentrations over the different streets of Paris range between 32 and 44 μg m^{-3} for NO_2, 1.4 to 2.4 μg m^{-3} for BC, 7 and 18 μg m^{-3} for $PM_{2.5}$ and 13 500 and 17 800 for PNC, with huge variations within the city (see Table 2).

### 4.2. Hybrid approach with the CHIMERE/ADMS chain over Paris

The Hybrid CHIMERE/ADMS chain was setup over Paris with and without data assimilation. The segments of the street network are the same as in section 3.1. Regional-scale concentrations are simulated with the CHIMERE model (Menut et al. 2021) at a 3 km x 3 km resolution, to which are superposed the local-scale concentrations simulated with the

Table 2
Modelled concentrations of NO_2, BC, $PM_{2.5}$, and PNC in the different cities for summer and winter. The "Mean" column corresponds to the averaged concentrations simulated taking into account the urban variabilities. The "min–max" column corresponds to the min and max time-averaged concentrations in the urban area.

		Concentrations (μg m^{-3} for NO_2, BC and $PM_{2.5}$ and #particles cm^{-3} for PNC)							
		NO_2		BC		$PM_{2.5}$		PNC	
		Mean	Min-max	Mean	Min-max	Mean	Min-max	Mean	Min-max
Paris Euler.	Summer	32.6	15.4–110	1.4	0.7 – 4.7	7.8	6.0–18.7	13,600	6,200–43,600
	Winter	43.8	27.6–117	2.4	1.3 – 8.4	17.5	13.1–33.9	17,900	8,300–72,900
Paris hybrid	Summer	30.6	18.6–69.6	2.2	1.4–5.9	9.0	7.2–22.2	–	–
	Winter	44.7	30.3–77.8	3.0	2.1–6.4	20.9	17.8–35.9	–	–
Paris hybrid assimilated	Summer	24.8	16.9–63.2	1.7	0.78–6.1	8.6	6.5–20.9	–	–
	Winter	35.0	27.9–66.3	1.7	0.85–5.6	14.4	12.1–27.8	–	–
Birmingham	Summer	14.6	7.8–91.1	–	–	6.9	5.9–16.5	2,400	2,200–4,100
	Winter	26.5	17.4–98.7	–	–	13.2	10.4–24.0	2,800	2,400–4,700
Athens	Summer	11.7	0.3–38.2	–	–	13.0	11.2–25.4	–	–
	Winter	12.7	0.8–39.5	–	–	13.2	9.8–27.0	–	–
Bucharest	Summer	29.2	18.0–56.9	–	–	12.7	9.3–19.1	26,200	15,300–42,000
	Winter	28.7	13.0–53.8	–	–	19.9	4.7–35.4	29,200	14,700–45,600
Rotterdam	Summer	14.0	7 – 58	1.2	0.5–2.9	–	–	23,300	13,700–119,100
	Winter	–	–	1.8	0.7–4.5	–	–	20,300	8,800–78,700
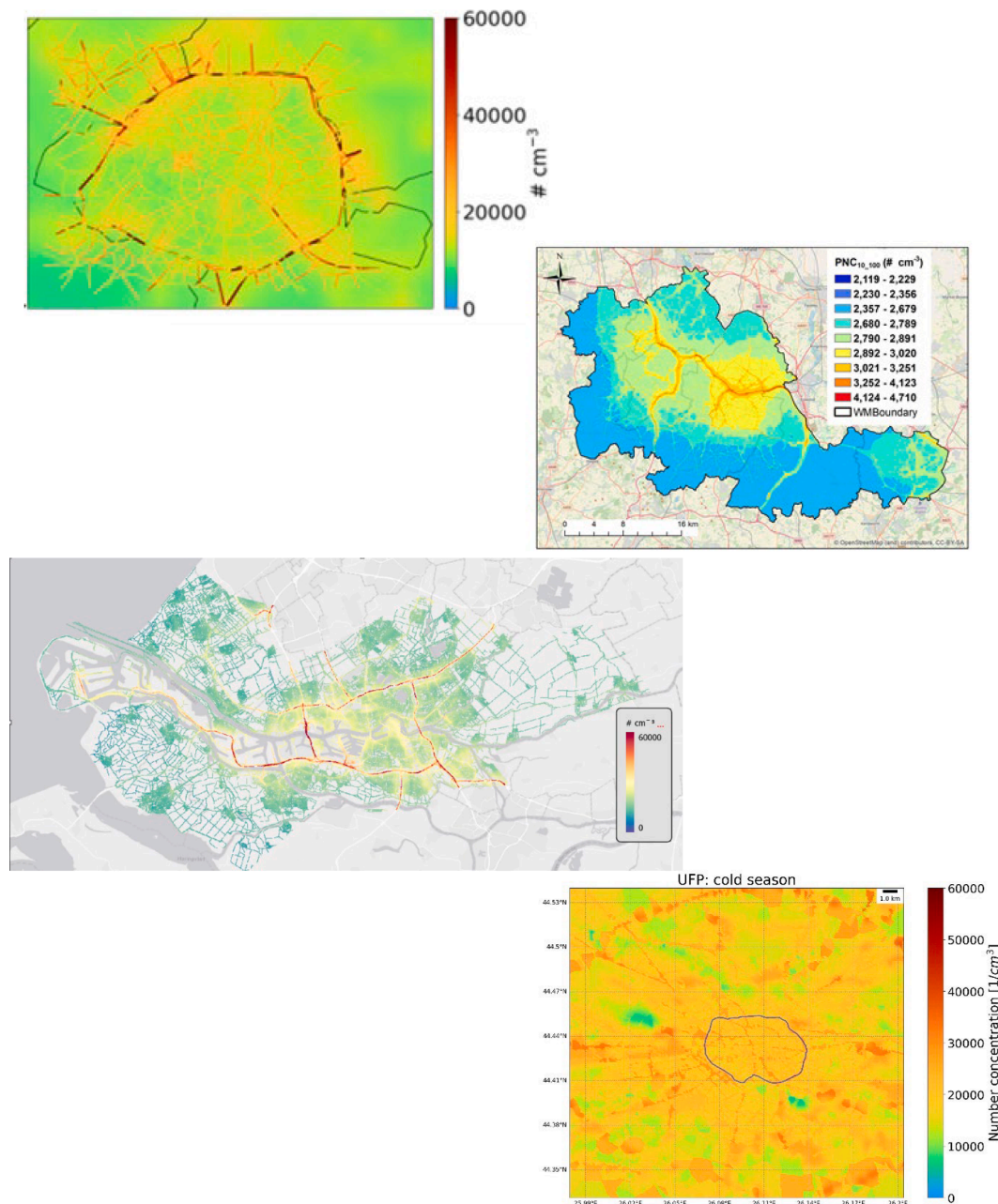
Fig. 3. Average PNC in #particles cm-3 over Paris (upper left panel), Birmingham (upper right panel), Rotterdam (lower left panel), Bucharest (lower right panel).

Gaussian-based model ADMS-Urban (Stocker et al. 2012). The concentrations of NO$_2$, PM$_{2.5}$ and BC are gridded at a 50 m x 50 m resolution. The boundary conditions of CHIMERE are obtained from CHIMERE simulations through PREV'AIR (https://www.prevair.org/). The bottom-up Aiparif inventory is used, and at the local scale, traffic fleet and emissions are specific to the period of simulation as in 3.1. For comparisons to observations, the simulated BC concentrations are obtained by multiplying the simulated EC concentrations by a harmonization factor, following Savadkoohi et al. (2024). The simulation was performed for June and July 2022 for the summer period, and January and February 2022 for the winter period. Although the summer period is the same as in 3.1, the winter period is a different year. It corresponds to the same year as the summer period (winter 2022), whereas winter 2020/2021 was chosen in 3.1 because of an intensive Airparif PNC measurement campaign that year.

The simulated concentrations at a 50 m x 50 m resolution are evaluated by comparison to measurement stations from the Airparif network. As detailed in Appendix A, the modelled concentrations satisfy the strictest performance criteria for NO$_2$, PM$_{2.5}$ and BC at background and traffic stations when data assimilation is not performed. NO$_2$ and BC concentrations are over-estimated at background sites, likely due to an overestimation of the background concentrations combined to the addition of both background and local contributions. Data assimilation systematically improves the error MFE and the FAC2 statistics. However, it sometimes leads to an increase in the bias MFB, especially at traffic stations for BC. This bias at traffic sites could be due to the limited number of stations at traffic sites for DA. Thus, the bias is higher for BC (only 2 to 3 traffic stations used for DA) than for NO$_2$ (9 stations used for DA). More observation stations would be needed for further improvements.

4.3. Hybrid approach with the EPISODE-CityChem model over Athens

The concentration variability of NO$_2$ and PM$_{2.5}$ in Athens was

assessed using the multi-scale numerical atmospheric model system CAMS/WRF/EPISODE-CityChem. The core of the system is the chemistry transport model EPISODE-CityChem (Karl et al. 2019, Lasne et al. 2023). Its comprehensive chemistry scheme is designed for treating complex atmospheric chemistry in urban areas and improved representation of the near-field dispersion. Emissions are provided by UrbEm (Ramacher et al., 2011), which disaggregates the regional CAMS database down to emission rates in 1 km resolution. In the frame of RI-URBANS, both tool and database have been refined (Kuenen et al., 2024). The model performs a specialized treatment on road and over the adjacent urban areas. Specifically, it is fed with hourly road network emissions in a linear format, applies a Gaussian dispersion scheme in the street canyons, and an extra photochemical scheme over the greater area of road surfaces, gridded in 100 m-by-100 m cells. These two schemes are superimposed to the Eulerian treatment of atmospheric processes in the whole 3D urban domain, with a horizontal spatial resolution of 1 km and a 24-layered atmosphere up to 3.7 km.

Local-scale atmospheric simulations are performed for 2019, which is a recent year, free of Covid-related activity restrictions, and with a wind field representative of 2016–2020. Numerical predictions have been evaluated against local air quality measurements from the National regulatory network and from the PANhellenic infrastructure for Atmospheric Composition and climatE change (PANACEA) Research Infrastructure (RI). The months used to represent summer are June, July, August and for winter they are December, January, February for winter.

The simulated concentrations (in 100 m cells) are evaluated by comparison with measurement stations. Four background and traffic stations are available to evaluate NO_2, one background station is available to evaluate $PM_{2.5}$ concentrations in summer, and two traffic stations are available to evaluate $PM_{2.5}$ concentrations in summer and winter. As detailed in Appendix A (Tables A.2.1 and A.2.2), the strictest performance criteria are met for NO_2 at traffic stations in summer and winter, the less strict criteria are met for NO_2 at background stations in summer. NO_2 concentrations tend to be under-estimated by comparisons to measurements at urban background stations. For $PM_{2.5}$, the strictest criteria are met at background and traffic stations in summer and winter. In the simulation, the average concentrations over Athens range between 11 and 13 μg m^{-3} for NO_2, and are around 13 μg m^{-3} for $PM_{2.5}$, with huge variations within the city for NO_2 (see Table 2). The average modelled NO_2 concentrations of Table 2 are lower than those in Paris, although measurements at traffic and background sites are higher, probably because of the under-estimation of modelled NO_2 concentrations in the urban background.

4.4. Gaussian-based approach with the ADMS-Urban model over Birmingham

The local scale ADMS-Urban Gaussian plume air dispersion model has been used for the Birmingham Pilot to generate high resolution air quality datasets for NO_2, $PM_{2.5}$ and PNC (Zhong et al., 2021; Zhong et al., 2023). Meteorological parameters measured at Birmingham Airport synoptic meteorological site were applied to drive the atmospheric dispersion in the boundary layer in the model. Background concentration input files were derived based on measured air quality datasets from rural background sites (available via the UK Automatic Urban and Rural Network, AURN) surrounding the West Midlands region. The upwind background site for each hour over the year was selected based on the monitored wind direction at that hour for NO_2, and $PM_{2.5}$. For PNC, there is a limited number of AURN sites in the UK, and Chilbolton was considered as an appropriate rural background site to inform the modelling background. For NO_2 and $PM_{2.5}$, the emission inventories were derived based on the UK NAEI emissions at a spatial resolution of 1 km × 1 km. Unlike emission inventories for traditional air pollutants (e.g. NO_2 and $PM_{2.5}$), there are limited sources for the emission inventory for UFPs in the UK. Therefore, for particle number, the emission inventory developed in the RI-Urbans project with a 6 km × 6

km spatial resolution was taken as an input for gridded emissions in the ADMS-Urban model. For the explicit major road emissions, the local traffic model datasets for traffic activities, average speed and fleet composition have been obtained from Transport for West Midlands and Birmingham City Council. An Atmospheric Emissions Inventory Toolkit (EMIT developed by Cambridge Environmental Research Consultants, CERC) has been used to pre-process all types of emission sources before these can be formatted and used by the ADMS-Urban model. The advanced street canyon and urban canopy modules have been applied to consider local street canyon effect on reduced dispersion of air pollutants and urban canopy effect on larger scale atmospheric flow due to spatially varying roughness length. A novel task farming approach was adopted to optimise the computing time via the parallel running of on multiple cores on supercomputer clusters at the University of Birmingham. Simulations were for June, July and August 2019 (summer), and January, February and December 2019 (winter).

The simulated concentrations for receptor locations are evaluated by comparison to measured concentrations obtained from UK AURN and the BAQS supersites. Five background and three traffic stations are available to evaluate NO_2, four background and one traffic stations are available to evaluate $PM_{2.5}$, and one background station is available to evaluate PNC. The modelled concentrations satisfy the strictest performance criteria for NO_2 and $PM_{2.5}$ at both background and traffic stations in winter and summer, and the less strict performance criteria for PNC at the background station. The mean NO_2 concentrations are lower than Paris, but higher than Athens: they range between 13 and 29 μg m^{-3} for NO_2. Average concentrations of between 7 and 14 μg m^{-3} for $PM_{2.5}$ were lower than Paris and Athens (in summer), but equal to Athens in winter. The average PNC are at least 5 times lower than in Paris: the average ranges between 2,100 #particles cm^{-3} and 2,900 #particles cm^{-3}.

4.5. Mixed-effect LUR modelling over Rotterdam

A car was used to measure the ambient concentrations of NO_2, BC and PNC during two seasons; one in November-December 2022 and in May-July 2023. The car was equipped with lab-grade 1 Hz NO_2 (CAPS, Aerodyne Research Inc., USA), 1 Hz BC (AE33, Magee Scientific), and 1 Hz UFP (EPC 3783, TSI) monitors measuring simultaneously. UFP measurements include particles from 7 nm diameter. A Global Positioning System (GPS) (G-Star IV, GlobalSat, Taiwan) was used to record the location of the car, which was linked to the measuring equipment via date and time. The measurements were mainly carried out between 08.00 and 22.00 h every day in the study period (including some weekend days) covering all parts of the city. For NO_2, only summer measurements were available, due to malfunction of the equipment in the winter campaign.

The data was winsorised to the 2.5th and the 97.5th percentile. That is, measured concentration levels below the 2.5th percentile and above the 97.5th percentile were "replaced" by the respective percentile values (Kerckhoffs et al. 2022). This procedure is done to balance the undue influence of extreme values, while allowing very high pollution values. For averaging, the data was first assigned to the nearest street and aggregated over each 50-meter (min: 30 m and max: 60 m) street segment per individual drive day. In total about 40,000 street segments were measured (out of the 250.000 segments predicted in total).

The seasonal average concentrations over Rotterdam are about 14 in summer for NO_2, they ranged between 1.2 to 1.8 μg m^{-3} for BC, 20,300 and 23,300 #particles cm^{-3} for PNC, with huge variations within the city (see Table 2). Although the NO_2 concentrations are lower than in Paris, but higher than in Athens, the BC concentrations are similar to those in Paris, and the PNC are slightly higher, probably because PNC include particles from 7 nm diameter in Rotterdam, against from 10 nm in Paris.

As UFP is not often measured by fixed stations, we only evaluated the model performance of NO_2 and BC with fixed-stations (from DCMR) in the Appendix. For BC, the modelled concentrations are similar to the

fixed-site measurements during winter (when the AE33 was used), but they are over-estimated by a factor between 1.6 and 2 in summer (when the MA300 was used). These differences may be due to the differences in the instruments measuring BC at fixed-sited and with mobile data, as they were not corrected by a harmonization factor.

Mixed modelling followed the approach outlined in our earlier work (Kerckhoffs, 2022). Because of the smaller number of repeats per street-segment for the Rotterdam campaign compared to previous Amsterdam and Copenhagen campaigns, the LUR part of the model played a larger role. Furthermore, we did not drive all streets segments, so application of the mixed model only included the fixed part for non-monitored street segments.

4.6. Mixed-effect LUR modeling over Bucharest

Mobile measurements campaigns representative for summer and winter periods have been conducted in Bucharest on a 100 km route. The route included representative areas for the city, among them heavily trafficked roads inside the city and residential, industrial and commercial areas, as well as sub-urban areas. Portable and high-time resolution instruments for UFP (Naneos Partector 2, 1 s), measuring particles from 10 nm diameter, different particle matter fractions ($PM_{2.5}$, PM_{10}) and gaseous compounds (NO_2) (Ecomesure EcomTrek − 10 s and/or Snif-fer4D V2, 1 s) have been used during both campaigns. The car measurements campaigns took place during two seasons: 04 May –13 July 2022 (summer period) and 18 January −28 February 2023 (winter period). A GPS (Navilock NL-442U, 1 s) was used to independently save the geographic coordinates. For averaging, the data was first assigned to the middle point of the street segment and aggregated over each 250-meter (min: 232 and max: 250 m) street segment per individual drive day. In total, 19,530 street segments were measured.

The measurement route has been designed to pass main sectors and areas representative of Bucharest city, with a total length of around 100 km. The measurements durations were approximately 8 h starting from 8:30 AM local time in order to catch rush hours, but also less intense traffic during the mid-day of working days. At least a full 15 measurements routes were performed during each campaign, in different temperature conditions. The quality control of the data included data filtration to remove the spikes, but keeping pollution related values if they are valid for several consecutive measurements. The filtering used a moving average window on 3 datapoints, the concentrations higher and lower by more 1.5 times than the mean values being removed.

The ESCAPE Land Use Regression model (Schmitz et al., 2019) together with PyLUR tool and QGIS (Ma et al, 2020) was first set up. Then the mixed effect model was implemented, using the mean value from the fixed effect model together with the pollutant variability (intercept of mean standard deviation values) for all individual street segments at 1 min. Individual maps for each pollutant at 100 m x100 m grid have been retrieved for each season (Talianu et al., 2024).

The model performance has been evaluated for NO_2 and PM_{10} concentrations using the hourly data available at the Romanian National Air Quality Monitoring Network (8 fixed stations representative for urban, industrial and suburban areas) and at the RADO-Bucharest ACTRIS site (Nicolae et al., 2010). The mean NO_2 concentration is close to the observed one for the winter period, but it is overestimated by a factor 1.6 during the summer period. However, the mean NO_2 concentration of the modelled data is within the variability of the measurements, given by the standard deviation. For PM_{10}, the mean concentration is close to the observed one for both the winter and the summer periods. The average concentrations over Bucharest range between 28 and 29 µg m^{-3} for NO_2, 12 to 19 µg m^{-3} for $PM_{2.5}$. The PNC are higher than in Paris and Rotterdam: between 26,200 and 29,200 #particles cm^{-3} (see Table 2). Although the same LUR modelling technique is used in Rotterdam and Bucharest, particles from 10 nm are measured in Bucharest and 7 nm in Rotterdam. Thus, the differences might not arise from the model, but

they might be due to differences in traffic fleet composition between cities or to a larger influence of industrial sites. Fixed site measurements of PNC are thus desirable to confirm these differences.

5. Seasonal and spatial variability

The seasonal and spatial variability are detailed for the different pollutants. The seasonal changes are driven by changes in pollutant sources (e.g. heating), as well as atmospheric conditions with lower boundary layer heights in winter. The spatial changes are driven by the presence of localized sources (e.g. traffic or industrial), and they are strongly dependent on the lifetime of the pollutant.

Because different methodologies are employed to model the variability within the studied European cities, that may influence the capacity to get similar variability to the observed one at measurement sites. Also, a bias on the modelling of concentrations at either background or traffic stations may lead to a bias in the variability. The spatial variabilities at fixed measurement sites, i.e. the modelled and observed variabilities between background and traffic stations are compared in Fig. 4 for NO_2 and $PM_{2.5}$ and in Fig. 5 for BC. The seasonal variabilities from urban background and traffic stations are compared in Fig. 6 for NO_2 and $PM_{2.5}$ and in Fig. 7 for BC and PNC. For NO_2 and $PM_{2.5}$, the MPI is also provided in the Figures. When comparisons are available, the MPI is lower than 1, corresponding to a satisfying representation of the variability in the models. The NSD values are also summarized in the Table of Appendix C. The spatial variabilities integrated over cities for summer and winter are shown in Fig. 8.

### 5.1. Influence of the mapping methodology on the variability

For the spatial variability estimated using fixed measurement sites, the NO_2 and BC variabilities tend to be similar and higher than the $PM_{2.5}$ variability. For NO_2, the seasonal variability tends to be lower than the spatial variability, while for $PM_{2.5}$, the seasonal and spatial variability are of the same order. Less data is available for BC and PNC. For BC, the seasonal variability is higher than the spatial one in Rotterdam, but lower in Paris. The PNC seasonal variability at urban background sites is very low in Paris, but higher in Rotterdam. The influence of the mapping methodology on the estimation of the variability is now first examined for cities using the LUR methodology and then for cities using deterministic modelling.

For cities using the LUR methodology, the seasonal variability is underestimated (for NO_2 in Bucharest and BC in Rotterdam). For the spatial variability, in Rotterdam, the NSD of BC based on measurements is similar to the modelled one in winter (0.13 for the modelled one and 0.14 for the observed one), and lower by 38 % in summer. However, the simulated spatial variability of NO_2 is much lower than the observed one in Bucharest (lower by 70 % to 80 %). As the mobile car measurements are done on roads, a large number of roads with different typologies may be required to estimate well the background concentrations and hence the variability between background and traffic stations. The number of sampled streets performed with mobile measurements is indeed higher in Rotterdam (40 000) than in Bucharest (about 20 000) for a similar land-surface area. This indicates that sampling a large number of streets could lead to better estimation of the background concentrations and of the variability using mobile measurements. Note that the statistical strength of the analysis is limited as there is only one NO_2 measuring station available at a traffic site in Bucharest during winter.

For cities using deterministic modelling, the representation of the spatial and seasonal variability varies depending on the methodology. The seasonal variability tends to be underestimated in Athens, but well represented in Birmingham. The seasonal variability is well modelled at background sites in Paris, but overestimated at traffic sites.

In the Paris Eulerian methodology (CHIMERE/MUNICH), the modelled spatial NSD of NO_2 is similar to the modelled one in summer (0.45 for the modelled one and 0.47 for the observed one), and higher by
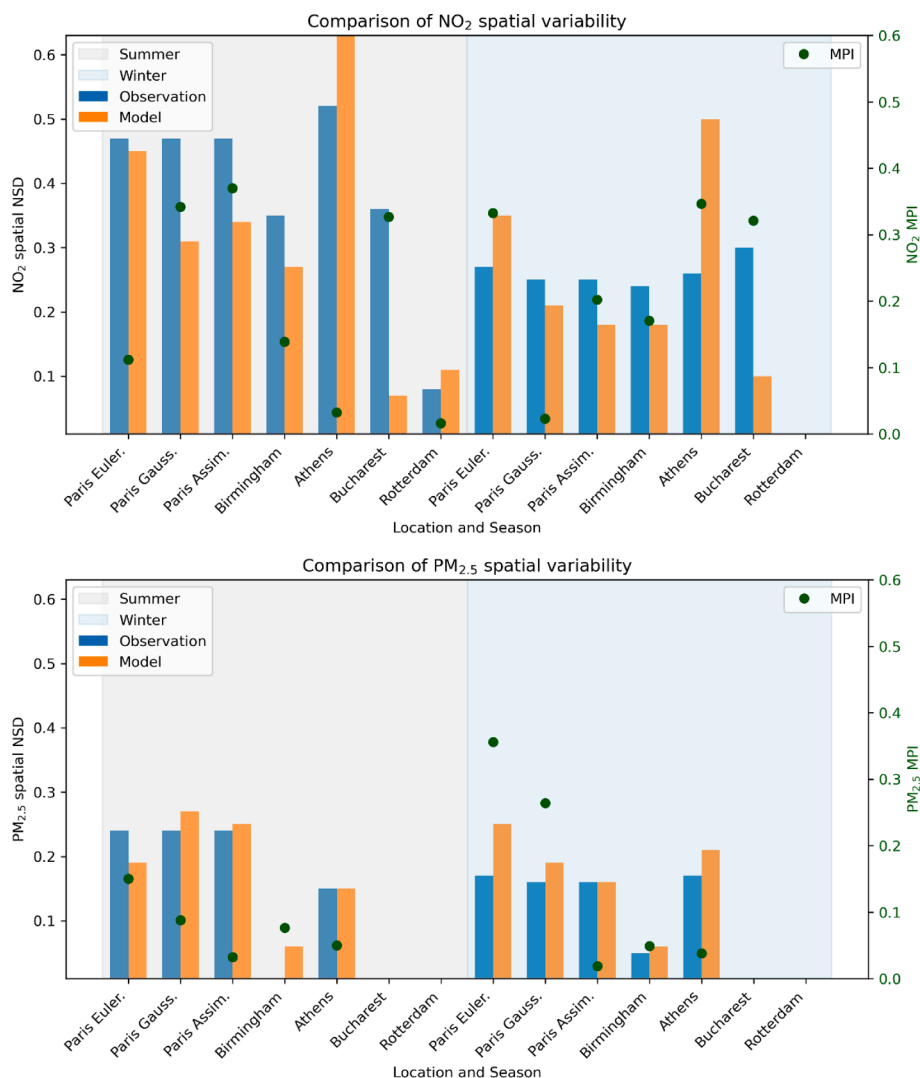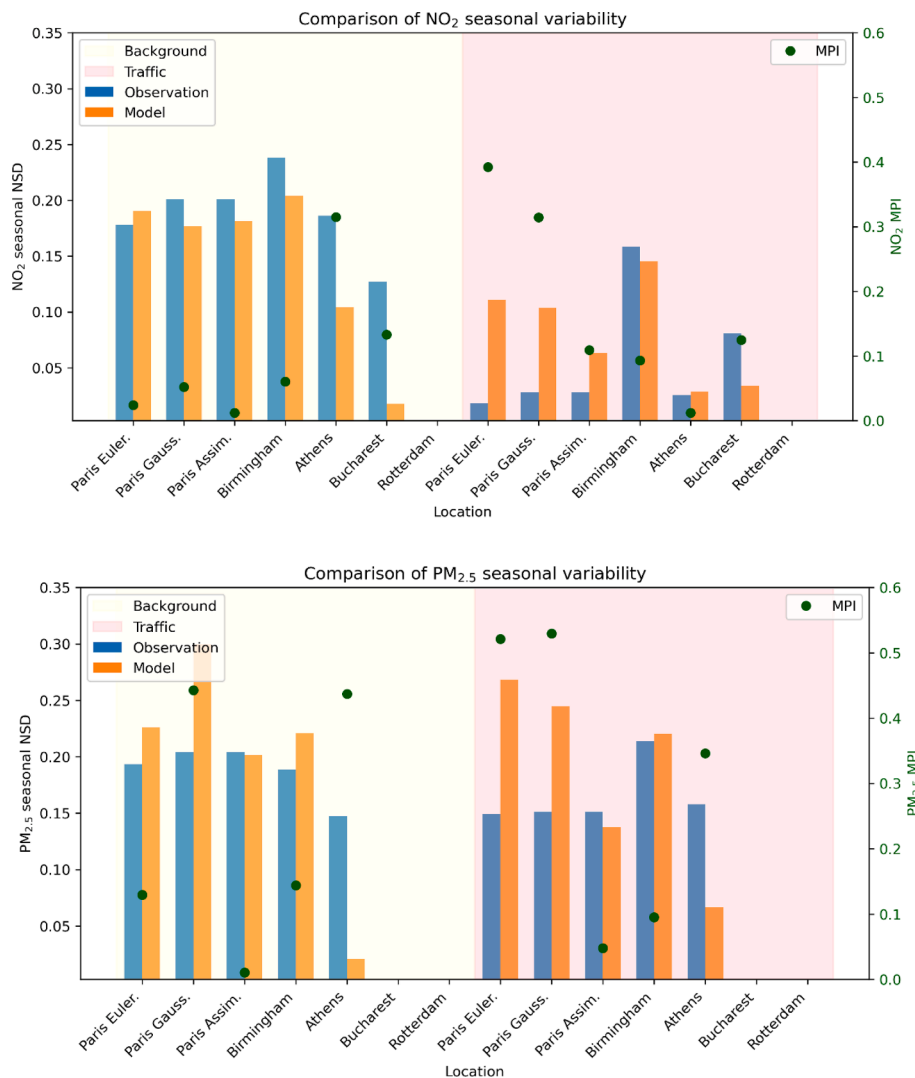
Fig. 4. Comparisons for summer and winter of NO$_2$ (upper panel) and PM$_{2.5}$ (lower panel) modelled spatial NSD to the spatial NSD estimated from measurements at background and traffic stations. The model performance indicator MPI quantifies the differences between model and measurements.
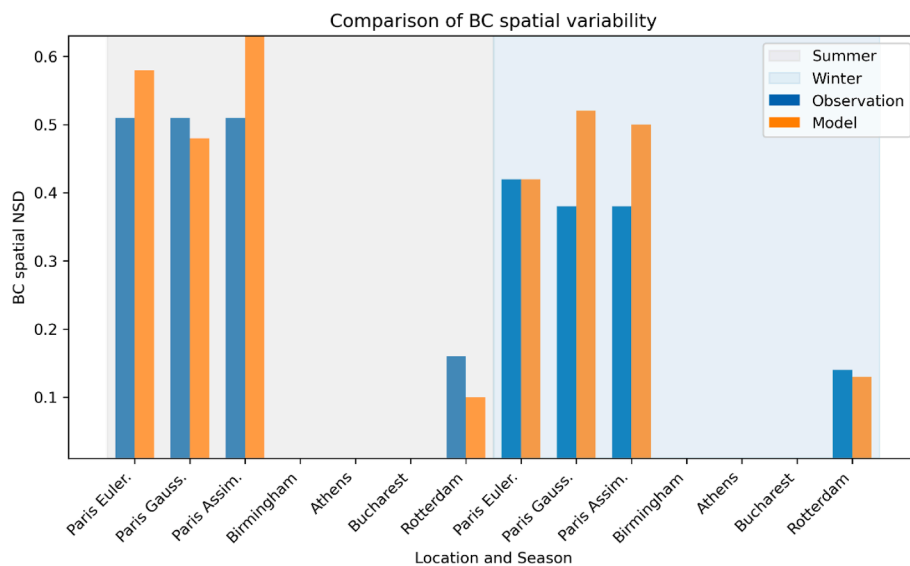
Fig. 5. Comparisons for summer and winter of BC modelled spatial NSD to the spatial NSD estimated from measurements at background and traffic stations.

Fig. 6. Comparisons at background and traffic sites of NO_2 (upper panel) and $PM_{2.5}$ (lower panel) modelled seasonal NSD to the seasonal NSD estimated from measurements during winter and summer. The model performance indicator MPI quantifies the differences between model and measurements.

30 % in winter. The modelled spatial NSD of BC is very similar to the modelled one in both winter and summer (0.51/0.42 for the modelled ones in summer/winter respectively and 0.55/0.42 for the observed ones). The differences are higher for $PM_{2.5}$: the observed NSDs are lower/higher than the modelled one by 20 %/47 % in summer/winter. These differences are due to an underestimation/overestimation of concentrations at traffic sites in summer/winter. The numbers of traffic stations for BC and $PM_{2.5}$ are much lower than for NO_2, limiting the strength of the analysis.

In the Paris hybrid methodology (CHIMERE/ADMS), the modelled spatial NSD of NO_2 is underestimated by 34 % and 16 % in the summer and the winter. As Gaussian concentrations are superposed to the Eulerian ones in the approach used over Paris, the background concentrations are over-estimated especially for NO_2, reducing the differences between the urban background and street concentrations. This is improved by data assimilation (DA), which does slightly increase the variability in summer, and improve the statistics in terms of errors between simulated and observed concentrations (MFE and FAC2 in Appendix A). However, this improvement of variability using DA is not systematic, because DA tends to lead to an underestimation of average concentrations of NO_2 at traffic stations (greater negative bias at traffic stations with DA), thus underestimating the differences between background and streets. Hence, DA improves the representation of the

variability in summer (27 % difference with the observations against 34 % without), but degrades it in winter (28 % difference with the observations against 16 % without). For BC, the NSD is well modelled in summer without DA, but it is over-estimated in the winter by 37 % without DA and 32 % with DA. DA does not always improve the modelling of the variability: in summer, the NSD of BC is less well represented with than without DA (24 % over-estimation with DA and 6 % under-estimation without). For $PM_{2.5}$, the modelled NSD is over-estimated by 13 % and 18 % in summer and winter, and it is much better represented with DA, with less than 4 % difference between the observed and modelled ones.

Over Athens, the modelled spatial NSD of NO_2 is over-estimated by 24 % in summer and 92 % in winter. For both seasons, the over-estimation is due to an under-estimation of NO_2 concentrations at background stations. The variability of $PM_{2.5}$ is better modelled, with an under-estimation of 12 % in summer and an over-estimation of 24 % in winter.

Over Birmingham, the modelled spatial NSD of NO_2 is under-estimated by 33 % in the summer and 25 % in the winter. For $PM_{2.5}$, the spatial NSD is well modelled in summer, but over-estimated by a factor 6 in winter. This large difference should be treated with caution, as there is only one $PM_{2.5}$ measuring station at a traffic site, limiting the statistical strength of the analysis.
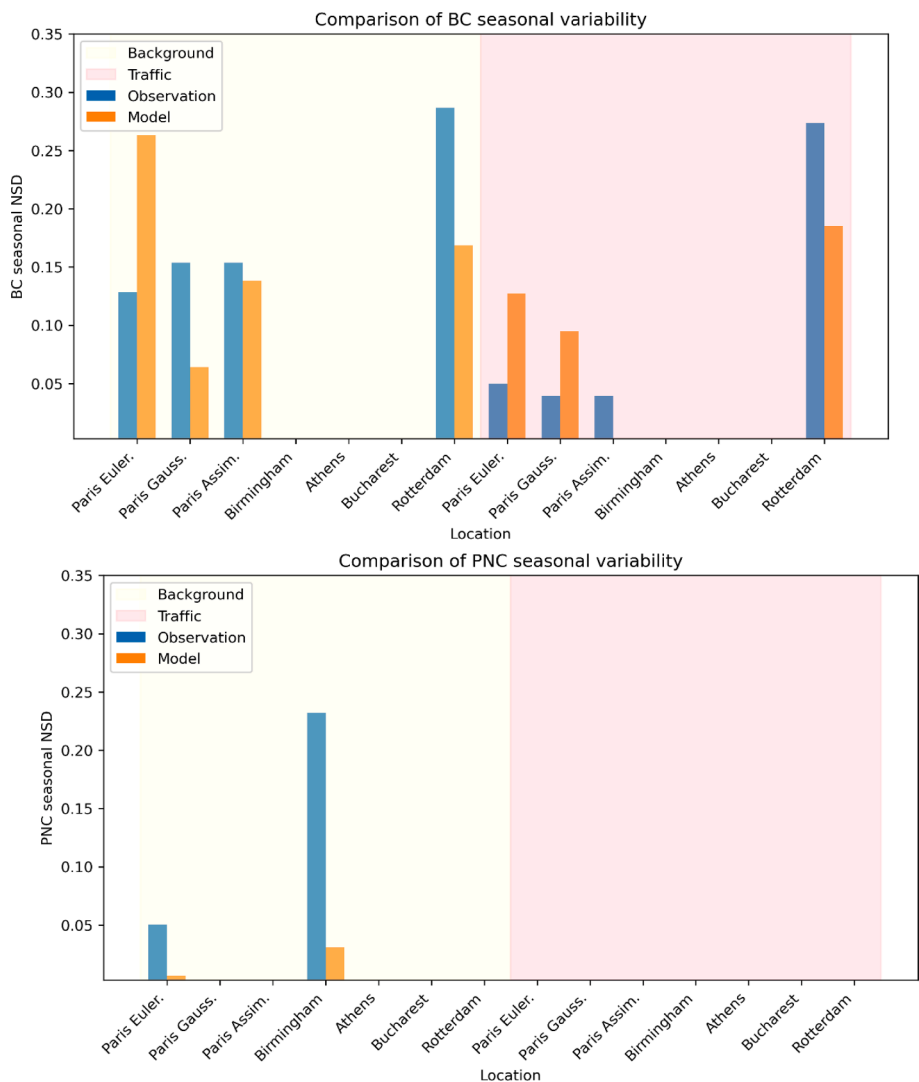
Fig. 7. Comparisons at background and traffic sites of BC (upper panel) and PNC (lower panel) modelled seasonal NSD to the seasonal NSD estimated from measurements during winter and summer.
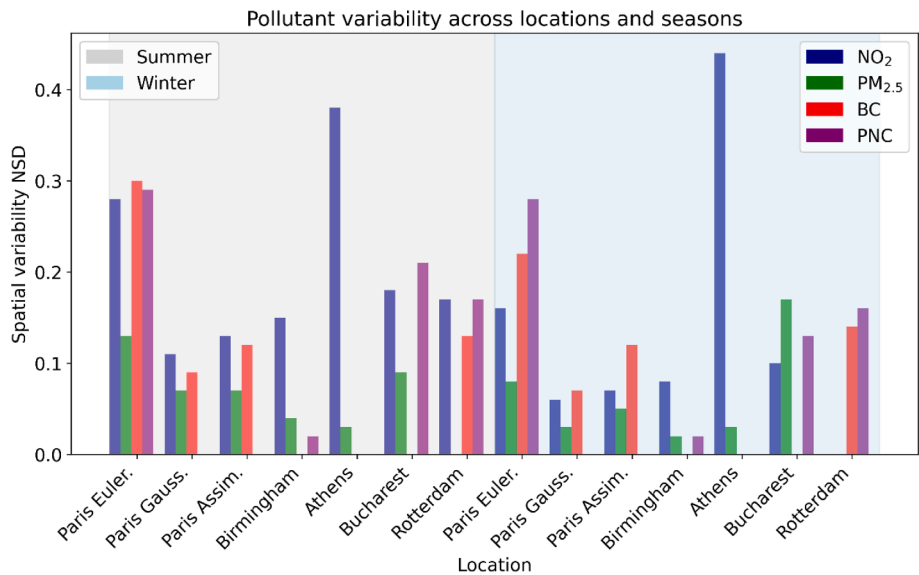

Fig. 8. Modelled pollutant variability across locations and seasons integrated over the different cities.

5.2. Analyses of the spatial variability

In both winter and summer, the concentrations of NO_2 are higher on streets than in the urban background, and the concentrations are the highest along streets with high traffic in all pilot cities. For example, high NO_2 concentrations are observed along the ring road in Paris and Bucharest. High concentrations are observed in the center of cities. As for NO_2, concentrations of BC, PNC and $PM_{2.5}$ are also high along roads and in the city center, but the contrast is not always as systematic for $PM_{2.5}$. As shown in Fig. 1, which shows the PNC concentrations for a winter period over Rotterdam, Bucharest, Birmingham, Paris, the PNC gradients over short distances are significant, with for example differences up to a factor of 2 in the mean in Bucharest. In Rotterdam, the major roads in and around the city have the highest concentrations. This is more pronounced on the highways for PNC than for NO_2 and BC. PNC are associated with UFPs. They quickly transform through physico-chemical processes, like coagulation or condensation and can reach background levels within 300 m of a highway, with even sharper gradients for the smaller particles. Concentrations are not only high along traffic routes and agglomerations, but also in industrial areas, where pronounced concentrations of PNC and PM are depicted in Bucharest. Away from major roads and in rural areas, concentrations are generally lower for all the pollutants studied.

For NO_2, the largest NSD at stations are observed in Athens and Paris, and they are very similar (0.49 in Athens and 0.47 in Paris for the observed NSDs in summer). In Paris, the integrated variability modelled using the coupled Gaussian-Eulerian approach (CHIMERE-ADMS) is much lower than the Eulerian one (CHIMERE/MUNICH) (0.11 against 0.28), in agreement with the lowest variabilities simulated by CHIMERE/ADMS at the measurement stations. This lower integrated variability using the local Gaussian modelling may be partly due to the assumption of homogeneity on which Gaussian models are based, and partly due to differences in the integration of the variability (over streets for CHIMERE/MUNICH and over 50 m x 50 m grid for CHIMERE/ADMS). The observed NSD at stations are similar for Birmingham, and Bucharest, but lower than Athens and Paris (0.35 in Birmingham, 0.36 in Bucharest, 0.47 in Paris and 0.49 in Athens). Except for the simulated NSD in Athens in winter, which seems to have a bias due to an underestimation of background concentrations, the winter NSDs are lower than the summer ones (for example 0.49 in summer and 0.26 in winter for the observed NSDs in Athens), indicating that diffuse sources of NO_2, such as residential heating by gas, may reduce the variability in winter.

For NO_2, BC, $PM_{2.5}$ and PNC, the NSD is higher in places with large roads. For example, the NSD is 0.28 in Paris for NO_2, but reaches 0.39 when calculated for the cells that host the Paris ring road, with high traffic. For NO_2, BC and PNC, the differences between winter and summer are lower near to the Paris ring road than within Paris, reflecting the strong influence of traffic near large roads all year along.

For $PM_{2.5}$, for almost all cities and cases, the NSD is much lower than for NO_2, by about a factor varying between 1.5 and 4, reflecting the large regional background of $PM_{2.5}$ compared to NO_2. The exception is Bucharest in winter, as the modelled city NSD is higher for $PM_{2.5}$ (0.17) than for NO_2 (0.10). The higher NSD values are located outside of the city center (Fig. B7 of Appendix), indicating the potentially large influence of industrial sources on the winter time variability in connection with lower boundary layer.

For BC, the NSDs tend to be similar to NO_2. They are slightly lower than those of NO_2 in Rotterdam in summer (0.13 for the city modelled NSD for BC and 0.17 for NO_2). However, in Paris the NSDs of BC are higher than those of NO_2, for both the NSDs at stations and those modelled using Paris Euler. The difference between the two cities could be attributed to a higher contribution of traffic with a higher fraction of diesel vehicles in Paris, or to emissions from ships in Rotterdam having a less significant influence on urban variability compared to the impact of road traffic. Furthermore, in Rotterdam, the variability of BC remains consistent across seasons (0.14 in winter and 0.13 in summer). In

contrast, Paris shows lower BC variability during winter (with NSD values of 0.51 in summer and 0.42 in winter for observed NSD at stations, and 0.30 in summer and 0.22 in winter for city modelled NSD using the Paris Euler model). This reduced wintertime variability in Paris may result from residential heating emissions, with wood burning for heating being more prevalent in Paris than Rotterdam (Zauli-Sajani et al. 2024).

For PNC, the NSD is similar to the NSD of BC in summer in Paris and Rotterdam, and it is similar or higher than the NSD of NO_2 in Bucharest, Rotterdam and Paris. The very low values of NSD in Birmingham for PNC may be due to an artefact, such as an underestimation of local emissions, uncertainties in background representation, or the lack of aerosol dynamics in the model. Another factor affecting Birmingham is the very small number of street canyon locations, although this might be expected to affect all traffic-generated pollutants similarly. Recent measurements of NSD in Birmingham for total PNC are higher than the model predictions, and closer to the values for the other cities in this study. The most probable explanation would be that road traffic emission factors were too low, which would also explain the small spatial variability predicted by the model in comparison to that in the other cities. As for NO_2, the NSDs of PNC and BC are especially large near large roads or near industrial sources. For example, the NSD is 0.28 in Paris in summer, but 0.39 in cells that include the Paris ring road. Although the NSD of NO_2 is clearly lower in winter than in summer, the wintertime NSD of PN is sometimes smaller but mostly similar with its summer value, e.g. 0.29 and 0.28 in Paris, and 0.17 and 0.16 in Rotterdam, in summer and winter, respectively. In Bucharest, higher PN variability is modelled in the summer (0.21) than in the winter (0.13). Wood burning emissions may have a low influence on the emissions of ultrafine particles, as the diameters of the emitted particles tend to be higher than 0.1 μ m. However, depending on the environment, the largest concentrations of $PM_{2.5}$ in the winter time could lead to enhanced coagulation of ultrafine particles, reducing their concentrations compared to summer time.

5.3. Analyses of the seasonal variability

For NO_2, the concentrations are higher in winter than in summer in Birmingham and in the urban background of Paris and Athens. However, they are similar at traffic sites in Paris and Athens and in Athens city center. The higher urban background NO_2 concentrations in Athens and Paris may be linked to lower boundary layer height during winter than summer, decreasing the volume in which city emissions are diluted. The influence may not be seen at traffic stations, because NOx emissions are for a large part emitted by traffic and as NO. The NO emissions are transformed into NO_2 locally by reaction with ozone. Photochemistry, which leads to ozone formation, is higher in summer than in winter, leading to higher local-NO_2 production in summer, more pronounced in the southern cities, e.g. Athens, which partly explains the higher summer (than winter) concentrations at the traffic sites. However, concentrations in streets are also influenced by the urban background. Hence, the higher local-NO_2 production in summer is counterbalanced by the higher urban background NO_2 in winter, leading to small seasonal differences at the traffic sites. As seen in the NO_2 maps of Bucharest or Paris, the NO_2 concentration presents a higher gradient during summer, when the concentrations are higher on the main roads. The concentrations are less street-confined during winter.

For BC and $PM_{2.5}$, concentrations are higher in winter than in summer, probably because the boundary layer height is lower and the atmosphere may have greater stability occurrence due to the lower temperatures in winter, leading to an accumulation of anthropogenic pollutants emitted in the city. Also, during the winter season, the contributions of residential emissions from heating tend to increase particle concentrations. In both Rotterdam and Paris, the BC concentrations are more than 1.5 times higher in winter than in summer, respectively 1.8 µg m^{-3} and 1.2 µg m^{-3} in Rotterdam and 2.4 µg m^{-3} and 1.4 µg m^{-3} in

Paris. The higher BC concentrations in the winter can potentially partly be attributed by wood smoke, as elevated concentrations are seen in the suburbs as well. In winter, the difference in concentration between the background and street concentrations seems relatively lower compared to summer.

For PNC, concentrations are higher in winter in Paris, Birmingham and Bucharest, but the concentrations are similar in winter and summer in Rotterdam. In Rotterdam, the concentrations are on average slightly higher in summer than in winter, respectively 23.000 #particles cm^{-3} and 20.000 #particles cm^{-3}, probably because of secondary particle formation (Gani et al. 2021). This can be expected with a large port and industrial cluster emitting SOx and NOx that will likely act as PNC precursors. In Bucharest, particle concentrations present higher loadings during the winter period, with decreased gradients, but gradients due to point sources linked to industries can still be distinguished. The lower differences between summer and winter for PNC than for PM$_{2.5}$ and BC could be partly due to wood heating, which tends to emit particles of diameter higher than 80 nm (Garcia-Marlès et al. 2024), and partly due to enhanced coagulation of freshly emitted UFP with pre-existing fine particles, which have higher concentrations in winter.

6. Discussion

This study mapped air pollutants with large urban concentration gradients over Paris, Athens, Rotterdam, Birmingham, Bucharest, utilizing several techniques, based on empirical or deterministic modelling. Depending on the method used, data may not be obtained for all pollutants (NO$_2$, PM$_{2.5}$, black carbon BC and particulate number concentrations PNC for UFP). The concentrations mapped using the different approaches are compared to measurements performed at fixed stations. Modelled concentrations are compared at urban background sites and traffic sites when possible. Inter-season and inter-pollutant variability in each city are evaluated, highlighting the similarities among cities or representative pollutants levels distribution for some of them. For cities using the mixed-LUR approach, such as Bucharest and Rotterdam, the comparison focuses on seasonal mean concentrations and their spatial variations. For cities using deterministic modelling, more detailed statistics of comparisons, such as hourly concentrations are computed. The concentrations maps retrieved using Land-Use-Regression model rely on mobile measurements, which are quantitatively limited and are representative for measurements conditions, such as time of the day, weekdays or weekend, and season. Deterministic modeling, on the other hand, relies on physical and chemical models that simulate how pollutants are emitted, dispersed, chemically transformed, and deposited, using detailed meteorological data, emission inventories, and atmospheric physics. Hence, deterministic models can capture day-to-day or even hour-to-hour variability, providing a detailed temporal resolution of pollutant behavior. Comparisons at several types of stations and multiple time periods (or seasons) allow for an increased confidence in the model ability to accurately map the pollutant concentrations and variability. A bias in the ability to represent a typology of stations leads to an error in the variability estimation.

The variability is characterized here by a normalized standard deviation (NSD). The differences in NSD values integrate across cities are likely influenced not only by local pollution sources and climatic conditions but also by the tools used to characterize the variability. Hence, the variability between background and traffic stations is also estimated, to allow comparisons between the modelled variability and the variability measured at fixed stations. Modelling based on LUR needs to include measurements from a large-enough number of streets in the network. They tend to underestimate the seasonal variability. Gaussian approaches tend to smooth out variability in urban areas. With deterministic modelling, aerosol dynamics need to be accounted for in order to represent the variability of ultrafine particles. For efficient data assimilation algorithms, there is the need to have sufficient number of stations representative of the different environments. Typically, over

Paris, 2 to 3 traffic stations for BC have proven insufficient, and lead to large bias at traffic sites.

The variabilities of NO$_2$, BC and PNC are between 1.5 and 4 times larger than those of PM$_{2.5}$, except in locations with industrial sites, reflecting the large background and variety of sources of PM$_{2.5}$ compared to the other pollutants for which the influence of traffic emissions is strong. For PNC, NO$_2$, BC, and PM$_{2.5}$, the variability is high in areas close to large roads. The variability of NO$_2$ and PM$_{2.5}$ tends to be larger in summer than in winter, as other area sources such as residential heating may reduce the variability in winter. For BC, the winter variability may be reduced by wood burning. The variability of PNC and BC tends to be similar in summer, and to be similar or higher than that of NO$_2$. Although the variability of NO$_2$ is clearly lower in winter than in summer, the variability of PNC is almost always similar for winter and summer, as residential heating may tend to emit particles of larger diameter than traffic. For NO$_2$, BC and PNC, the differences between winter and summer are lower near large roads, under strong traffic influence.

7. Conclusion

The study quantifies intra-urban air pollution variability across five European cities (Paris, Athens, Birmingham, Rotterdam, and Bucharest) with a fine resolution (<100 m) for regulated and emerging pollutants (NO$_2$, PM$_2$. $_5$, black carbon, and ultrafine particles), emphasizing differences in pollution drivers such as traffic and residential heating emissions. Different state-of-the-art air pollution mapping techniques (empirical and deterministic modeling) are presented and their ability to capture this intra-urban spatial and seasonal variability is analyzed. A standardized methodology is defined to compare the mapping methods in terms of their accuracy in representing intra-urban air pollution patterns over space and time. Although the scarcity of fixed-site measurements at traffic sites and/or for BC and UFP limits the robustness of these comparisons, the modeled pollutant's spatial and seasonal variability is generally well represented across methodologies when compared to fixed-stations measurements. The deterministic modeling approaches (e.g., Eulerian or Gaussian dispersion models) are most effective when fine-scale emission inventories and urban morphological information are available, allowing an hourly representation of concentrations. They are well suited for NO$_2$ and PM$_2$. $_5$, and the Eulerian multi-scale model represents well both UFP and BC. The comparison also shows that better emission source characterization of UFP is essential for improving deterministic mapping capabilities. Land-use regression models based on mobile monitoring provide a valuable approach for seasonal concentrations, in places where mobile monitoring data are dense, allowing detailed mapping of both UFP and BC.

To facilitate comparisons, a metric was introduced to enable cross-pollutant comparisons (NO$_2$, PM$_2$. $_5$, BC, and UFP). The variability of BC and UFP was shown to be at least as high as the variability of NO$_2$. This has important implications for exposure assessment and policy, emphasizing the need for operational implementation over cities of fine-scale mapping techniques to enhance population exposure estimation and public health evaluations, particularly for NO$_2$, UFP, and BC. This study demonstrates that the variability integrated across a city differs significantly depending on whether it is estimated from a few fixed monitoring stations or across the entire domain, independently of the modelling technique used. Multi-scale modeling is hence essential to accurately assess population exposure, and more urban and traffic fixed-site measurements are needed, especially for UFP and BC, to support further refinement of models.

In addition to the presentation and evaluation of modeling techniques, the influence of data assimilation on the intra-urban variability representation is analyzed. While data assimilation improves model to measurement comparisons of concentrations, it does not always enhance variability representation between traffic and urban background sites, emphasizing the need for more advanced assimilation approaches, in

particular to improve predictions of pollutants for which observations are scarce.

Future research should focus on comparing mapping techniques capable of representing all pollutants of interest within the same city and expanding their application across multiple cities to better assess population exposure to highly variable pollutants.

8. Model availability

- The code of the CHIMERE/MUNICH/SSH-aerosol chain may be obtained from https://zenodo.org/records/12639507.
- The code of the EPISODE-CityChem model may be obtained from: https://zenodo.org/records/8063985.
- The code of the ADMS model (for case studies) needs a model licence from Cambridge Environmental Research Consultants (https://www.cerc.co.uk/environmental-software/ADMS-Urban-model.html).
- The LUR model for Bucharest was developed locally using the ESCAPE Land Use Regression model manual, available online: https://escapeproject.eu/; https://www.escapeproject.eu/manuals/

CRediT authorship contribution statement

Karine Sartelet: Writing – review & editing, Writing – original draft, Visualization, Validation, Supervision, Software, Resources, Project administration, Methodology, Funding acquisition, Formal analysis, Conceptualization. **Jules Kerckhoffs:** Writing – review & editing, Writing – original draft, Visualization, Validation, Software, Resources, Methodology, Investigation, Formal analysis. **Eleni Athanasopoulou:** Writing – review & editing, Writing – original draft, Visualization, Validation, Software, Resources, Methodology, Investigation, Formal analysis. **Lya Lugon:** Writing – review & editing, Visualization, Validation, Software, Resources, Methodology, Investigation, Formal analysis. **Jeni Vasilescu:** Writing – review & editing, Writing – original draft, Visualization, Validation, Software, Resources, Methodology, Investigation, Formal analysis. **Jian Zhong:** Writing – review & editing, Writing – original draft, Visualization, Validation, Software, Resources, Methodology, Investigation, Formal analysis. **Gerard Hoek:** Writing – review & editing, Writing – original draft, Visualization, Validation, Supervision, Resources, Project administration, Methodology, Investigation, Funding acquisition, Formal analysis, Conceptualization. **Cyril Joly:** Writing – review & editing, Writing – original draft, Validation, Software, Methodology, Investigation, Formal analysis. **Soo-Jin Park:** Writing – review & editing, Visualization, Validation, Software, Investigation, Formal analysis. **Camelia Talianu:** Writing – review & editing, Visualization, Validation, Software, Investigation, Formal analysis. **Sef van den Elshout:** Supervision. **Fabrice Dugay:** Writing – review & editing, Validation, Resources, Methodology, Investigation, Conceptualization. **Evangelos Gerasopoulos:** Validation, Supervision, Resources. **Alexandru Ilie:** Validation, Software, Investigation, Formal analysis. **Youngseob Kim:** Software, Data curation. **Doina Nicolae:** Funding acquisition, Conceptualization. **Roy M. Harrison:** Writing – review & editing, Supervision, Funding acquisition, Conceptualization. **Tuukka Petäjä:** Writing – review & editing, Supervision, Project administration, Funding acquisition, Conceptualization.

Declaration of competing interest

The authors declare that they have no known competing financial interests or personal relationships that could have appeared to influence the work reported in this paper.

Acknowledgements

Appendix A. Supplementary data

Supplementary data to this article can be found online at https://doi.org/10.1016/j.envint.2025.109474.

Data availability

Data will be made available on request.

References

Adélaïde, L., Medina, S., Wagner, V., de Crouy-Chanel, P., Real, E., Colette, A., Couvidat, F., Bessagnet, B., Alter, M., Durou, A., Host, S., Hulin, M., Corso, M., Pascal, M., 2021. Covid-19 lockdown in spring 2020 in France provided unexpected opportunity to assess health impacts of falls in air pollution. Front. Sust. Cities 3, 643821. https://doi.org/10.3389/frsc.2021.643821.

Apte, J.S., Manchanda, C., 2024. High-resolution urban air pollution mapping. Science 385, 380–385. https://doi.org/10.1126/science.adq3678.

Berkowicz, R., 2000. OSPM – A parameterised street pollution model. Environ. Monit. Assess. 65, 323–331. https://doi.org/10.1023/A:1006448321977.

Bouma, F., Janssen, N.A.H., Wesseling, J., van Ratingen, S., Strak, M., Kerckhoffs, J., Gehring, U., Hendricx, W., de Hoogh, K., Vermeulen, R., Hoek, G., 2023. Long-term exposure to ultrafine particles and natural and cause-specific mortality. Environ. Int. 175, 107960. https://doi.org/10.1016/j.envint.2023.107960.

Boylan, J.W., Russell, A.G., 2006. PM and light extinction model performance metrics, goals, and criteria for three-dimensional air quality models. Atmos. Environ. 40 (26), 4946–4959. https://doi.org/10.1016/j.atmosenv.2005.09.087.

Brauer, M., et al., 2024. Global burden and strength of evidence for 88 risk factors in 204 countries and 811 subnational locations, 1990–2021: a systematic analysis for the Global Burden of Disease Study 2021. The Lancet 403, 2162–2203. https://doi.org/10.1016/S0140-6736(24)00933-4.

Cohen, A.J., Brauer, M., Burnett, R., Anderson, H.R., Frostad, J., Estep, K., Balakrishnan, K., Brunekreef, B., Dandona, L., Dandona, R., Feigin, V., Freedman, G., Hubbell, B., Jobling, A., Kan, H., Knibbs, L., Liu, Y., Martin, R., Morawska, L., Pope III, C.A., Shin, H., Straif, K., Shaddick, G., Thomas, M., van Dingenen, R., van Donkelaar, A., Vos, T., Murray, C.J.L., Forouzanfar, M.H., 2017. Estimates and 25-year trends of the global burden of disease attributable to ambient air pollution: an analysis of data from the Global Burden of Diseases Study 2015. Lancet 389, 1907–1918. https://doi.org/10.1016/S0140-6736(17)30505-6.

Colette, A., Collin, G., Besson, F., Blot, E., Guidard, V., Meleux, F., Royer, A., Petiot, V., Miller, C., Fermond, O., Jeant, A., Adani, M., Arteta, J., Benedictow, A., Bergström, R., Bowdalo, D., Brandt, J., Briganti, G., Carvalho, A. C., Christensen, J. H., Couvidat, F., D'Elia, I., D'Isidoro, M., Denier van der Gon, H., Descombes, G., Di Tomaso, E., Douros, J., Escribano, J., Eskes, H., Fagerli, H., Fatahi, Y., Flemming, J., Friese, E., Frohn, L., Gauss, M., Geels, C., Guarnieri, G., Guevara, M., Guion, A., Guth, J., Hänninen, R., Hansen, K., Im, U., Janssen, R., Jeoffrion, M., Joly, M., Jones, L., Jorba, O., Kadantsev, E., Kahnert, M., Kaminski, J. W., Kouznetsov, R., Kranenburg, R., Kuenen, J., Lange, A. C., Langner, J., Lannuque, V., Macchia, F., Manders, A., Mircea, M., Nyiri, A., Olid, M., Pérez García-Pando, C., Palamarchuk, Y., Piersanti, A., Raux, B., Razinger, M., Robertson, L., Segers, A., Schaap, M., Siljamo, P., Simpson, D., Sofiev, M., Stangel, A., Struzewska, J., Tena, C., Timmermans, R., Tsikerdekis, T., Tsyro, S., Tyuryakov, S., Ung, A., Uppstu, A., Valdebenito, A., van Velthoven, P., Vitali, L., Ye, Z., Peuch, V.-H., and Rouïl, L., 2024. Copernicus Atmosphere Monitoring Service – Regional Air Quality Production System v1.0, EGUsphere [preprint], doi: 10.5194/egusphere-2024-3744.

de Meij, A., Cuvelier, C., Thunis, P., and Pisoni, E., 2025. A new set of indicators for model evaluation complementing to FAIRMODE's MQO, EGUsphere [preprint], doi: 10.5194/egusphere-2024-3690.

Denby, B.R., Gauss, M., Wind, P., Mu, Q., Grøtting Wærsted, E., Fagerli, H., Valdebenito, A., Klein, H., 2020. Description of the uEMEP_v5 downscaling approach for the EMEP MSC-W chemistry transport model. Geosci. Model Dev. 13, 6303–6323. https://doi.org/10.5194/gmd-13-6303-2020.

European Environment Agency, 2018. CORINE Land Cover (CLC) 2018 dataset. Data file. URL: https://www.eea.europa.eu/publications/COR0-landcover. accessed: 2024-02-26.

Fernandes, A., Rafael, S., Lopes, D., Coelho, S., Borrego, C., Lopes, M., 2021. The air pollution modelling system URBAIR: how to use a Gaussian model to accomplish high spatial and temporal resolutions. Air Qual. Hlth. 14, 1969–1988. https://doi.org/10.1007/s11869-021-01069-9.

Gani, S., Chambliss, S.E., Messier, K.P., Lunden, M.M., Apte, J.S., 2021. Spatiotemporal profiles of ultrafine particles differ from other traffic-related air pollutants: lessons from long-term measurements at fixed sites and mobile monitoring. Environ. Sci.: Atmos., 1, 558–568. https://doi.org/10.1039/D1EA00058F.

Garcia-Marlès M., Lara R., Reche C., Pérez N., Tobías A., Savadkoohi M., Beddows D., Salma I., Vörösmarty M., Weidinger T., Hueglin C., Mihalopoulos N., Grivas G., Kalkavouras P., Ondracek J., Zikova N., Niemi J.V., Manninen H.E., Green D.C., Tremper A.H., Norman M., Vratolis S., Diapouli E.,Eleftheriadis K., Gómez-Moreno F.J., Alonso-Blanco E., Wiedensohler A., Weinhold K., Merkel M., Bastian S., Hoffmann B., Altug H., Petit J.-E., Acharja P., Favez O., Dos Santos S.M., Putaud J.-P., Dinoi A., Contini D., Casans A., Casquero-Vera J.A., Crumeyrolle S., Bourrianne E., Van Poppel M., Dreesen F.E., Harni S., Timonen H., Lampilahti J.,Petäjä T., Pandolfi M., Hopke P.K., Harrison R.M., Alastuey A., Querol X., 2024. Source apportionment of ultrafine particles in urban Europe, Environ. Int., 194, 109149, doi: 10.1016/j.envint.2024.109149.

Goobie, G.C., Saha, P.K., Carlsten, C., Gibson, K.F., Johannson, K.A., Kass, D.J., Ryerson, C.J., Zhang, Y., Robinson, A.L., Presto, A.A., Nouraie, S.M., 2024. Ambient Ultrafine Particulate Matter and Clinical Outcomes in Fibrotic Interstitial Lung Disease. Am. J. Respir. Crit. Care Med. 209 (9), 1082–1090. https://doi.org/10.1164/rccm.202307-1275OC.

Hamer, P.D., Walker, S.-E., Sousa-Santos, G., Vogt, M., Vo-Thanh, D., Lopez-Aparicio, S., Schneider, P., Ramacher, M.O.P., Karl, M., 2020. The urban dispersion model EPISODE v10.0 – Part 1: An Eulerian and sub-grid-scale air quality model and its application in Nordic winter conditions. Geosci. Model Dev. 13, 4323–4353. https://doi.org/10.5194/gmd-13-4323-2020.

Hanna, S., Chang, J., 2012. Acceptance criteria for urban dispersion model evaluation. Meteorol. Atmos. Phys. 116, 133–146. https://doi.org/10.1007/s00703-011-0177-1.

Hatzopoulou, M., Valois, M.F., Levy, I., Mihele, C., Lu, G., Bagg, S., Minet, L., Brook, J., 2017. Robustness of land-use regression models developed from mobile air pollutant measurements. Environ. Sci. Technol. 51 (7), 3938–3947. https://doi.org/10.1021/acs.est.7b00366.

Hoek, G., 2017. Methods for Assessing Long-Term Exposures to Outdoor Air Pollutants. Curr. Envir. Health Rpt., 4 (4), 450–462. https://doi.org/10.1007/s40572-017-0169-5.

Hood, C., Mackenzie, I., Stocker, J., Johnson, K., Carruthers, D., Vieno, M., Doherty, R., 2018. Air quality simulations for London using a coupled regional-to-local modelling system. Atmos. Chem. Phys. 18, 11221–11245. https://doi.org/10.5194/acp-18-11221-2018.

Hood, C., Stocker, J., Seaton, M., Johnson, K., O'Neill, J., Thorne, L., Carruthers, D., 2021. Comprehensive evaluation of an advanced street canyon air pollution model. J. Air Waste Manage. Assoc. 71, 247–267. https://doi.org/10.1080/10962247.2020.1803158.

Janssen, S., Thunis, P., 2022. FAIRMODE Guidance Document on Modelling Quality Objectives and Benchmarking (version 465 3.3), EUR 31068 EN, Publications Office of the European Union, JRC129254,https://fairmode.jrc.ec.europa.eu/document/fairmode/WG1/Guidance_MQO_Bench_vs3.3_20220519.pdf, doi: 10.2760/41988.

Jerrett, M., Arain, A., Kanaroglou, P., Beckerman, B., Potoglou, D., Sahsuvaroglu, T., Morrison, J., Giovis, C., 2005. A review and evaluation of intraurban air pollution exposure models. J. Expo. Anal. Environ. Epidemiol., 15 (2), 185–204. https://doi.org/10.1038/sj.jea.7500388.

Karl, M., Walker, S.-E., Solberg, S., Ramacher, M.O.P., 2019. The Eulerian urban dispersion model EPISODE – Part 2: Extensions to the source dispersion and photochemistry for EPISODE–CityChem v1.2 and its application to the city of Hamburg. Geosci. Model Dev. 12, 3357–3399. https://doi.org/10.5194/gmd-12-3357-2019.

Kerckhoffs, J., Hoek, G., Portengen, L., Brunekreef, B., Vermeulen, R.C., 2019. Performance of prediction algorithms for modeling outdoor air pollution spatial surfaces. Environ. Sci. Tech. 53 (3), 1413–1421. https://doi.org/10.1021/acs.est.8b06038.

Kerckhoffs, J., Khan, J., Hoek, G., Yuan, Z., Ellermann, T., Hertel, O., Ketzel, M., Jensen, S.S., Meliefste, K., Vermeulen, R., 2022a. Mixed-Effects Modeling Framework for Amsterdam and Copenhagen for Outdoor NO2 Concentrations Using Measurements Sampled with Google Street View Cars. Environ. Sci. Technol. 56 (11), 7174–7184. https://doi.org/10.1021/acs.est.1c05806.

Kerckhoffs, J., Khan, J., Hoek, G., Yuan, Z., Hertel, O., Ketzel, M., Jensen, S.S., Al Hasan, F., Meliefste, K., Vermeulen, R., 2022b. Hyperlocal variation of nitrogen dioxide, black carbon, and ultrafine particles measured with Google Street View cars in Amsterdam and Copenhagen. Environ Int. 170, 107575. https://doi.org/10.1016/j.envint.2022.107575.

Kerckhoffs, J., Hoek, G., Vermeulen, R., 2024. Mobile monitoring of air pollutants; performance evaluation of a mixed-model land use regression framework in relation to the number of drive days. Environmental Research 240, 117457. doi:doi: 10.1016/j.envres.2023.117457.

Kim, Y., Lugon, L., Maison, A., Sarica, T., Roustan, Y., Valari, M., Zhang, Y., André, M., Sartelet, K., 2022. MUNICH v2.0: a street-network model coupled with SSH-aerosol (v1.2) for multi-pollutant modelling. Geosci. Model Dev. 15, 7371–7396. https://doi.org/10.5194/gmd-15-7371-2022.

Kuenen, J., Athanasopoulou, E., Guevara, M., 2024. Emission inventories for regional and urban scale modelling applications. RI-URBANS Report. https://riurbans.eu/wp-content/uploads/2024/07/ST15_Emissions.pdf.

Lasne, J., Lostier, A., Salameh, T., Athanasopoulou, E., Karagiannis, D., Kakouri, A., Vassaux, S., Lesueur, D., Romanias, M.N., 2023. NOx emissions by real-world fresh and old asphalt mixtures: Impact of temperature, relative humidity, and UV-irradiation. Urban Climate 49, 101457. https://doi.org/10.1016/j.uclim.2023.101457.

Lequy, E., Siemiatycki, J., de Hoogh, K., Vienneau, D., Dupuy, J.-F., Garès, V., Hertel, O., Christensen, J.H., Zhivin, S., Goldberg, M., Zins, M., Jacquemin, B., 2021. Contribution of Long -Term Exposure to Outdoor BC to the Carcinogenicity of Air Pollution. Environ. Health Perspect. 129 (3), 37005. https://doi.org/10.1289/EHP8719.

Lequy, E., Leblond, S., Siemiatycki, J., Meyer, C., Vienneau, D., de Hoogh, K., Zins, M., Goldberg, M., Jacquemin, B., 2023. Long-term exposure to airborne metals and risk of cancer in the French cohort Gazel. Environ. Int. 177, 107999. https://doi.org/10.1016/j.envint.2023.107999.

Lin, C., Wang, Y., Ooka, R., Flageul, C., Kim, Y., Kikumoto, H., Wang, Z., Sartelet, K., 2023. Modeling of street-scale pollutant dispersion by coupled simulation of chemical reaction, aerosol dynamics, and CFD. Atmos. Chem. Phys. 23, 1421–1436. https://doi.org/10.5194/acp-23-1421-2023.

Lin, C., Ooka, R., Kikumoto, H., Flageul, C., Kim, Y., Zhang, Y., Sartelet, K., 2024. Impact of solid road barriers von reactive pollutant dispersion in an idealized urban canyon: A large-eddy simulation coupled with chemistry. Urban Climate 55, 101989. https://doi.org/10.1016/j.uclim.2024.101989.

Lloyd, M., Ganji, A., Xu, J., Venuta, A., Simon, L., Zhang, M., Saeedi, M., Yamanouchi, S., Apte, J., Hong, K., Hatzopoulou, M., Weichenthal, S., 2023. Predicting spatial variations in annual average outdoor ultrafine particle concentrations in Montreal and Toronto, Canada: Integrating land use regression and deep learning models. Environ. Int. 178, 108106. https://doi.org/10.1016/j.envint.2023.108106.

Lugon, L., Sartelet, K., Kim, Y., Vigneron, J., Chrétien, O., 2021. Simulation of primary and secondary particles in the streets of Paris using MUNICH. Faraday Discuss. 226, 432–456. https://doi.org/10.1039/D0FD00092B.

Lugon, L., Kim, Y., Vigneron, J., Chrétien, O., André, M., André, J.-M., Moukhtar, S., Redaelli, M., Sartelet, K., 2022. Effect of vehicle fleet composition and mobility on outdoor population exposure: A street resolution analysis in Paris. Atmos. Poll. Res. 13 (5), 101365. https://doi.org/10.1016/j.apr.2022.101365.

Ma, X., Longley, I., Salmond, J., Gao, J., 2020. PyLUR: Efficient software for land use regression modeling the spatial distribution of air pollutants using GDAL/OGR library in Python. Front. Environ. Sci. Eng. 14 (3), 44. https://doi.org/10.1007/s11783-020-1221-5.

Ma, X., Zou, B., Deng, J., Gao, J., Longley, I., Xiao, S., Guo, B., Wu, Y., Xu, T., Xu, X., Yang, X., Wang, X., Tan, Z., Wang, Y., Morawska, L., Salmond, J., 2024. A comprehensive review of the development of land use regression approaches for modeling spatiotemporal variations of ambient air pollution: A perspective from 2011 to 2023. Environ. Int. 183, 108430. https://doi.org/10.1016/j.envint.2024.108430.

Maison, A., Flageul, C., Carissimo, B., Tuzet, A., Sartelet, K., 2022a. Parametrization of Horizontal and Vertical Transfers for the Street-Network Model MUNICH Using the CFD Model Code_Saturne. Atmosphere 13, 527. https://doi.org/10.3390/atmos13040527.

Maison, A., Flageul, C., Carissimo, B., Wang, Y., Tuzet, A., Sartelet, K., 2022b. Parameterizing the aerodynamic effect of trees in street canyons for the street network model MUNICH using the CFD model Code_Saturne. Atmos. Chem. Phys. 22, 9369–9388. https://doi.org/10.5194/acp-22-9369-2022.

Martin, F., Janssen, S., Rodrigues, V., Sousa, J., Santiago, J., Rivas, E., Stocker, J., Jackson, R., Russo, F., Villani, M., Tinarelli, G., Barbero, D., José, R.S., Pérez-Camanyo, J., Santos, G.S., Bartzis, J., Sakellaris, I., Horvath, Z., Környei, L., Liszkai, B., Kovacs, A., Jurado, X., Reiminger, N., Thunis, P., Cuvelier, C., 2024. Using dispersion models at microscale to assess long-term air pollution in urban hot spots: A FAIRMODE joint intercomparison exercise for a case study in Antwerp. Sci. Tot. Environ., 925, 171761. https://doi.org/10.1016/j.scitotenv.2024.171761.

Menut, L., Bessagnet, B., Briant, R., Cholakian, A., Couvidat, F., Mailler, S., Pennel, R., Siour, G., Tuccella, P., Turquety, S., Valari, M., 2021. The chimere v2020r1 online chemistry-transport model. Geosci. Model Dev. 14 (11), 6781–6811. https://doi.org/10.5194/gmd-14-6781-2021.

Moin, P., Mahesh, K., 1998. DIRECT NUMERICAL SIMULATION: A Tool in Turbulence Research. Annu. Rev. Fluid Mech. 30, 539–578. https://doi.org/10.1146/annurev.fluid.30.1.539.

Nicolae, D., Vasilescu, J., Carstea, E., Stebel, K., Prata, F., 2010. Romanian Atmospheric Research 3D Observatory: Synergy of instruments. Rom. Rep. Phys. 62, 838–853.

OpenStreetMap, 2021. Openstreetmap database [postgresql via api]. © OpenStreetMap contributors. Available under the Open Database Licence from: https://openstreetmap.org. Data mining by Overpass turbo. Available at https://overpass-turbo.eu.

Park, M., Joo, H.S., Lee, K., Jang, M., Kim, S.D., Kim, I., Borlaza, L.J.S., Lim, H., Shin, H., Chung, K.H., Choi, Y.-H., Park, S.G., Bae, M.-S., Lee, J., Song, H., Park, K., 2018. Differential toxicities of fine particulate matters from various sources. Sci. Rep. 8, 17007. https://doi.org/10.1038/s41598-018-35398-0.

Park, S.J., Lugon, L., Jacquot, O., Kim, Y., Baudic, A., D'Anna, B., Di Antonio, L., Di Biagio, C., Dugay, F., Favez, O., Ghersi, V., Gratien, A., Kammer, J., Petit, J.-E., Sanchez, O., Valari, M., Vigneron, J., Sartelet, K., 2025. Population exposure to outdoor NO2, black carbon, and ultrafine and fine particles over Paris with multi-scale modelling down to the street scale. Atmos. Chem. Phys., 25, 3363–3387. https://doi.org/10.5194/acp-25-3363-2025.

Patiño, W.R., Vlček, O., Bauerová, P., Belda, M., Bureš, M., Eben, K., Fuka, V., Geletič, J., Jareš, R., Karel, J., Keder, J., Krč, P., Radović, J., Řezníček, H., Šindelářová, A., Resler, J., 2024. On the suitability of dispersion models of varying degree of complexity for air quality assessment and urban planning. Build. Environ., 264, 111892. https://doi.org/10.1016/j.buildenv.2024.111892.

Ramacher, M.O.P., Kakouri, A., Speyer, O., Feldner, J., Karl, M., Timmermans, R., Denier van der Gon, H., Kuenen, J., Gerasopoulos, E., Athanasopoulou, E., 2021. The UrbEm Hybrid Method to Derive High-Resolution Emissions for City-Scale Air Quality Modeling. Atmosphere 12 (11), 1404. https://doi.org/10.3390/atmos12111404.

Ridolfo, S., Amato, F., Querol, X., 2024. Particle number size distributions and concentrations in transportation environments: a review. Environ. Int. 187, 108696. https://doi.org/10.1016/j.envint.2024.108696.

Rood, A.S., 2014. Performance evaluation of AERMOD, CALPUFF, and legacy air dispersion models using the Winter Validation Tracer Study dataset. Atmos. Environ. 89, 707–720. https://doi.org/10.1016/j.atmosenv.2014.02.054.

Salim, M., Buccolieri, R., Chan, A., Di Sabatino, S., 2011. Numerical simulation of atmospheric pollutant dispersion in an urban street canyon: Comparison between RANS and LES. J. Wind Eng. Ind. Aerod. 99 (2–3), 103–113. https://doi.org/10.1016/j.jweia.2010.12.002.

Sarica, T., Maison, A., Roustan, Y., Ketzel, M., Jensen, S.S., Kim, Y., Chaillou, C., Sartelet, K., 2023. Modelling concentration heterogeneities in streets using the street-network model MUNICH. Geosci. Model Dev., 16, 5281–5303. https://doi.org/10.5194/gmd-16-5281-2023.

Sartelet, K., Couvidat, F., Wang, Z., Flageul, C., Kim, Y.: SSH-Aerosol v1.1,, 2020. A Modular Box Model to Simulate the Evolution of Primary and Secondary Aerosols. Atmosphere 11, 525. https://doi.org/10.3390/atmos11050525.

Sartelet, K., Kim, Y., Couvidat, F., Merkel, M., Petäjä, T., Sciare, J., Wiedensohler, A., 2022. Influence of emission size distribution and nucleation on number concentrations over Greater Paris. Atmos. Chem. Phys. 22, 8579–8596. https://doi.org/10.5194/acp-22-8579-2022.

Sartelet, K., Wang, Z., Lannuque, V., Iyer, S., Couvidat, F., Sarica, T., 2024. Modelling molecular composition of SOA from toluene photo-oxidation at urban and street scales. Environ. Sci.: Atmos. 4 (8), 839–847. https://doi.org/10.1039/D4EA00049H.

Savadkoohi, M., Pandolfi, M., Favez, O., Putaud, J.-P., Eleftheriadis, K., Fiebig, M., Hopke, P.K., Laj, P., Wiedensohler, A., Alados-Arboledas, L., Bastian, S., Chazeau, B., María, Á.C., Colombi, C., Costabile, F., Green, D.C., Hueglin, C., Liakakou, E., Luoma, K., Listrani, S., Mihalopoulos, E., Marchand, E., Močnik, G., Niemi, J.V., Ondráček, J., Petit, J.-E., Rattigan, O.V., Reche, C., Timonen, H., Titos, G., Tremper, A.H., Vratolis, S., Vodička, P., Funes, E.Y., Zíková, N., Harrison, R.M., Petäjä, T., Alastuey, A., Querol, X., 2024. Recommendations for reporting equivalent black carbon (eBC) mass concentrations based on long-term pan-European in-situ observations. Environ. Int. 185, 108553. https://doi.org/10.1016/j.envint.2024.108553.

Schmitz, O., Beelen, R., Strak, M., Hoek, G., Soenario, I., Brunekreef, B., Vaartjes, I., Dijst, M.J., Grobbee, D.E., Karssenberg, D., 2019. High resolution annual average air pollution concentration maps for the Netherlands. Sci .data 6 (1), 190035. https://doi.org/10.1038/sdata.2019.35.

Schraufnagel, D.E., 2020. The health effects of ultrafine particles. Exp. Mol. Med. 52, 311–317. https://doi.org/10.1038/s12276-020-0403-3.

Soulhac, L., Garbero, V., Salizzoni, P., Mejean, P., Perkins, R.J., 2009. Flow and dispersion in street intersections. Atmos. Environ. 43 (18), 2981–2996. https://doi.org/10.1016/j.atmosenv.2009.02.061.

Southerland, V.A., Brauer, M., Mohegh, A., Hammer, M.S., van Donkelaar, A., Martin, R. V., Apte, J.S., Anenberg, S.C., 2022. Global urban temporal trends in fine particulate matter (PM2·5) and attributable health burdens: estimates from global datasets. Lancet Planet Health 6 (2), 139–146. https://doi.org/10.1016/S2542-5196(21)00350-8.

Squarcioni, A., Roustan, Y., Valari, M., Kim, Y., Sartelet, K., Lugon, L., Dugay, F., and Voitot, R. (2024): To what extent is the description of streets important in estimating local air-quality? A case study over Paris, EGUsphere [preprint], doi: 10.5194/egusphere-2024-1043.

Stocker, J., Hood, C., Carruthers, D., McHugh, C., 2012. ADMS-Urban: developments in modelling dispersion from the city scale to the local scale. Int. J. Environ. Pollut., vol. 50, No.1/2/3/4, 308–316. https://doi.org/10.1504/ijep.2012.051202.

Talianu, C., Vasilescu, J., Nicolae, D., Ilie, A., Dandocsi, A., Nemuc, A., Belegante, L., 2024. High-resolution air quality maps for Bucharest using Mixed-Effects Modeling Framework. Egusphere [preprint]. https://doi.org/10.5194/egusphere-2024-2930.

Tilloy, A., Mallet, V., Poulet, D., Pesin, C., Brocheton, F., 2013. BLUE-based NO_2 data assimilation at urban scale. J. Geophys. Res. Atmos., 118, 2031–2040. https://doi.org/10.1002/jgrd.50233.

Thouron, L., Kim, Y., Carissimo, B., Seigneur, C., Bruge, B., 2019. Intercomparison of two modeling approaches for traffic air pollution in street canyons. Urban Climate 27, 163–178. https://doi.org/10.1016/j.uclim.2018.11.006.

Valari, M., Menut, L., 2020. Transferring the heterogeneity of surface emissions to variability in pollutant concentrations over urban areas through a chemistry-transport model. Atmos. Environ., 44, 3229–3238. https://doi.org/10.1016/j.atmosenv.2010.06.001.

Wang, Y., Chang, J., Hu, P., Deng, C., Luo, Z., Zhao, J., Zhang, Z., Yi, W., Zhu, G., Zheng, G., Wang, S., He, K., Liu, J., Liu, H., 2024. Key factors in epidemiological exposure and insights for environmental management: Evidence from meta-analysis. Environ. Poll., 362, 124991. https://doi.org/10.1016/j.envpol.2024.124991.

World Health Organization, 2021. Review of evidence on health aspects of air pollution: REVIHAAP project: technical report, https://iris.who.int/bitstream/handle/10665/341712/WHO-EURO-2013-4101-43860-61757-eng.pdf?sequence=1.

World Health Organization, 2021b. WHO global air quality guidelines: particulate matter (PM2.5 and PM10), ozone, nitrogen dioxide, sulfur dioxide and carbon monoxide. World Health. Organization. https://iris.who.int/handle/10665/345329.

Zauli-Sajani, S., Thunis, P., Pisoni, E., Bessagnet, B., Monforti-Ferrario, F., De Meij, A., Pekar, F., Vignati, E., 2024. Reducing biomass burning is key to decrease PM2.5 exposure in European cities. Sci Rep. 14 (1), 10210. https://doi.org/10.1038/s41598-024-60946-2.

Zhong, J., Hood, C., Johnson, K., Stocker, J., Handley, H., Wolstencroft, M., Mazzeo, A., Cai, X., Bloss, W.J., 2021. Using task farming to optimize a street-scale resolution air quality model of the West Midlands (UK). Atmosphere 12 (8), 983. https://doi.org/10.3390/atmos12080983.

Zhong, J., Harrison, R.H., Bloss, W.J., Visschedijk, A., Gon, H.D.V., 2023. Modelling the dispersion of particle number concentrations in the West Midlands, UK using the ADMS-Urban model. Environ. Int. 181, 108273. https://doi.org/10.1016/j.envint.2023.108273.